# A pan-serotype dengue virus inhibitor targeting the NS3-NS4B interaction

Suzanne J. F. Kaptein[1], Olivia Goethals[2], Dominik Kiemel[3], Arnaud Marchand[4], Bart Kesteleyn[5], Jean-François Bonfanti[6,11], Dorothée Bardiot[4], Bart Stoops[5], Tim H. M. Jonckers[5], Kai Dallmeier[1], Peggy Geluykens[5,12], Kim Thys[5], Marjolein Crabbe[5], Laurent Chatel-Chaix[3,13], Max Münster[3], Gilles Querat[7], Franck Touret[7], Xavier de Lamballerie[7], Pierre Raboisson[5,14], Kenny Simmen[5], Patrick Chaltin[4,8], Ralf Bartenschlager[3,9], Marnix Van Loock[2*], Johan Neyts[1,10*]

[1]KU Leuven, Department of Microbiology, Immunology and Transplantation, Rega Institute for Medical Research, Laboratory of Virology and Chemotherapy, Herestraat 49, 3000 Leuven, Belgium

[2]Janssen Global Public Health, Janssen Pharmaceutica NV, Turnhoutseweg 30, 2340, Beerse, Belgium

[3]Department of Infectious Diseases, Molecular Virology, Heidelberg University, Im Neuenheimer Feld 344, Heidelberg 69120, Germany

[4]Cistim Leuven vzw, Bioincubator 2, Gaston Geenslaan 2, 3001 Leuven, Belgium

[5]Janssen Research & Development, Janssen Pharmaceutica NV, Turnhoutseweg 30, 2340, Beerse, Belgium

[6]Janssen Infectious Diseases Discovery, Janssen-Cilag, Chaussée du Vexin, 27106 Val de Reuil, France

[7]Unité des Virus Émergents (UVE: Aix-Marseille Univ–IRD 190–Inserm 1207–IHU Méditerranée Infection), Marseille, France

[8]Centre for Drug Design and Discovery (CD3), KU Leuven, Bioincubator 2, Gaston Geenslaan 2, 3001 Leuven, Belgium

[9]German Center for Infection Research, Heidelberg partner site, Heidelberg 69120, Germany

[10]Global Virus Network (GVN)

[11]Present address: Galapagos, 102 Avenue Gaston Roussel, 93230 Romainville, France

[12]Present address: Charles River Beerse, Discovery, Turnhoutseweg 30, 2340 Beerse, Belgium

[13]Present address: Institut National de la Recherche Scientifique, Centre Armand-Frappier Santé Biotechnologie, 531, Boulevard des Prairies Laval, Québec, QC H7V 1B7, Canada

[14]Present address: Aligos bvba, Bio-Incubator Leuven NV, Gaston Geenslaan 1, Leuven, Belgium

[*] Corresponding authors: johan.neyts@kuleuven.be and mvloock@its.jnj.com

**Dengue virus (DENV) causes ~96 million symptomatic infections annually, manifesting as dengue fever or occasionally as severe dengue[1,2]. There are no antivirals available to prevent or treat dengue. We describe a highly potent DENV inhibitor (JNJ-A07) that exerts nano- to picomolar activity against a panel of 21 clinical isolates, representing the natural genetic diversity of known geno- and serotypes. The molecule has a high barrier to resistance and prevents the formation of the viral replication complex by blocking the interaction between two viral proteins (NS3 and NS4B), thus unveiling an entirely novel mechanism of antiviral action. JNJ-A07 has an excellent pharmacokinetic profile that results in outstanding efficacy against DENV infection in mouse infection models. Delaying start of treatment until peak viremia results in a rapid and significant reduction in viral load. An analogue is currently in further development.**

## MAIN TEXT

Dengue is currently considered one of the top10 global health threats[1]. Annually, an estimated 96 million develop dengue disease[2], which is likely an underestimation[3-5]. The incidence has increased ~30-fold over the past 50 years. The virus is endemic in 128 countries in (sub-)tropical regions, with an estimated 3.9 billion people at risk of infection. A recent study predicts an increase to 6.1 billion people at risk by 2080[6]. The upsurge is driven by factors such as rapid urbanization and the sustained spread of the mosquito vectors[6-8]. DENV has four serotypes (further classified into genotypes), which are increasingly co-circulating in endemic regions. A second infection with a different serotype increases the risk of severe dengue[9,10]. The vaccine Dengvaxia®, which is approved in a number of countries for those aged ≥9 years, is only recommended for those with previous dengue exposure[11,12,13]. There are no antivirals for the prevention or treatment of dengue; the development of pan-serotype DENV inhibitors has proven challenging[14,15].

57 **JNJ-A07, a highly potent DENV inhibitor**

58 Following a large-scale cell-based anti-DENV-2 screen[16], a hit was identified and optimized (a
59 total of ~2,000 analogues were synthesized) to molecules, of which JNJ-A07 is a representative
60 analogue (Fig. 1a), with nano- to picomolar antiviral potency in various cell lines and with a high
61 selectivity (Table 1a, Extended Data Fig 1). JNJ-A07 is also active in primary immature dendritic
62 cells, which may be the initial target cells[17]. Potent pan-genotype and pan-serotype activity (nM
63 to pM potencies) was demonstrated against a panel of 21 clinical isolates covering all available
64 genotypes within the four serotypes[18] (Table 1b). No marked antiviral activity was detected against
65 other flaviviruses nor against a selection of other RNA and DNA viruses (Extended Data Fig. 2).

66 **JNJ-A07 targets the DENV NS4B protein**

67 Addition of JNJ-A07 to infected cultures could be delayed without loss of antiviral potency as long
68 as intracellular viral RNA synthesis had not been initiated up to a detectable level (at 10 hours post
69 infection [p.i.]; Extended Data Fig. 3a, b). When the inhibitor was added after onset of viral RNA
70 synthesis, a gradual loss of its antiviral activity was noted, suggesting an interaction with the viral
71 RNA replication machinery. A similar pattern was observed with the nucleoside analogue 7-deaza-
72 2'-*C*-methyladenosine, a broad-spectrum RNA virus inhibitor. To identify the molecular target,
73 drug-resistant variants were selected by passaging DENV-2 in the presence of gradually increasing
74 concentrations of JNJ-A07 (Extended Data Fig. 3c). This proved exquisitely difficult in two
75 independent efforts (A and B). As shown in the dynamics of appearance of mutations (Extended
76 Data Fig. 3d, e), a decrease in susceptibility to the drug (32-fold) was first observed at week 15 of
77 the selection process, and nearly 40 weeks were needed to obtain nearly complete loss of antiviral
78 activity. Multiple mutations were identified (following whole-genome sequencing) within the viral
79 non-structural protein 4B (NS4B) at endpoint of which L94F, T108I and T216N were present in
80 100% of the population in sample A, and V91A, L94F and T108I in 100% and F47Y, P104S and
81 T216P in <100% of the population in sample B (Figure 1b, c, Extended Data Fig. 3d-f). These
82 mutations were not present in the in parallel-passaged untreated cultures. A close analogue of JNJ-
83 A07 (Analogue 1; Extended Data Table 1) resulted in the same mutations V91A, L94F and T108I
84 at endpoint (week 29) (Extended Data Fig. 3f). Several resistance mutations occur only at a very
85 low frequency (i.e., ≤0.5% across all 4 serotypes) in clinical isolates (Extended Data Fig. 3g), but
86 none of these appear together. Threonine-137 (which appeared and disappeared during selection
87 experiments in sample A) is present in 3.5% of DENV-2 clinical isolates and in 100% of the

88 clinical isolates of the other serotypes but is considered a polymorphism as it does not alter the
89 antiviral susceptibility. F47Y, S85L, V91A, L94F, P104S and T216N/P are not present in the panel
90 of 21 clinical isolates used in this study. Isolates DENV-1/Malaysia, DENV-2/Martinique,
91 DENV-2/Thailand, DENV-3/H87 and DENV-3/Brazil carry 108I or 108A (Table 1b), which may
92 possibly explain the slightly decreased susceptibility of some of these viruses to JNJ-A07 as
93 compared to the other viruses from the same genotype.

94 To determine the replication fitness and inhibitor resistance caused by these mutations, they were
95 inserted separately into a sub-genomic DENV-2/16681 reporter replicon (Extended Data Fig. 4a).
96 The mutations resulted either in profound attenuation of replication (F47Y, S85L, P104S, T216N)
97 or did not affect replication (V91A, T108I, A137T, T216P) (Fig. 1d, Extended Data Fig. 4b), which
98 did not correlate with the level of resistance imposed by these mutations (Fig. 1e). L94F conferred
99 the highest level of resistance (950-fold) but surprisingly increased the replication fitness
100 compared to wild-type (WT). This mutation was carried by virus strains obtained at endpoint of
101 two independent resistance selection efforts, with the selected viruses having >50,000-fold
102 reduced sensitivity to JNJ-A07 (Extended Data Fig. 3d, e). Although drug-resistant virus retained
103 full replication competence in Vero E6 cells (Extended Data Fig. 4c), it hardly replicated in C6/36
104 mosquito cells (Extended Data Fig. 4d-f).

105 **JNJ-A07 blocks the NS3-NS4B interaction**

106 As the mutations mapped to NS4B, we studied the possible impact of JNJ-A07 on the NS3-NS4B
107 interaction. To this end, NS4B was expressed as part of the NS4A-2K-NS4B precursor[19] along
108 with the NS2B-NS3 protease-helicase complex. To facilitate NS4B-specific pull-down, a C-
109 terminal hemagglutinin affinity-tag ($HA^{Ct}$) was added to NS4B. Cells were transfected with
110 constructs encoding the selected resistance mutants or the A137T natural polymorphism. WT
111 NS4B and the Q134A mutant (known to abolish the NS3-NS4B interaction[20]) were respectively
112 the positive and negative control and non-HA-tagged NS4B the technical control. Ratios of NS4B-
113 HA and co-precipitated NS3 were measured by quantitative Western blot (Extended Data Fig.5a,
114 b). For WT NS4B, JNJ-A07 (~45× $EC_{50}$; 0.035μM) decreased co-captured NS3 by 95% (Fig. 1f,
115 g), demonstrating that it prevents the NS3-NS4B interaction. Consistently, almost complete drug-
116 induced loss of the NS3-NS4B interaction was observed with mutants S85L and A137T (Fig. 1g),
117 which confer rather low or no drug resistance, respectively (Fig. 1e). In contrast, the NS3-NS4B

118 interaction was barely affected by JNJ-A07 in case of the higher drug resistance mutants V91A,
119 L94F, T108I, and T216N (Fig. 1f, g). Using T108I and V91A as examples for respectively
120 moderate and strong JNJ-A07 resistance mutations, dose-response assays were performed
121 (Extended Data Fig. 5c-k). V91A and T108I increased the $EC_{50}$ of the NS3-NS4B interaction by
122 respectively a factor 41 and 9 compared with WT (Extended Data Fig. 5e, h-k), which is in line
123 with their impact on resistance in virus assays (Fig. 1e). Moreover, a dose-dependent decrease of
124 the 2K-NS4B cleavage intermediate was noted with the level of decrease following the level of
125 resistance (Extended Data Fig. 5f, h-k). To a lesser extent, this effect was also noticed for mature
126 NS4B (Extended Data Fig. 5g-k), indicating that JNJ-A07 slows down the cleavage kinetics of the
127 NS4A-2K-NS4B precursor (Extended Data Fig. 5l).
128 Next, the kinetics of JNJ-A07-induced loss of the NS3-NS4B interaction was studied (Extended
129 Data Fig. 6a, b). Addition at 4 h post-transfection significantly reduced amounts of NS3-NS4B
130 complexes whereas treatment starting at 24 h had no significant effect in samples that were
131 harvested shortly thereafter (1 h or 8 h) (Fig. 1h). Thus, a reduction becomes visible only at late
132 time points (harvest after 24 h) when newly formed NS3-NS4B complexes are detectable,
133 suggesting that JNJ-A07 prevents the formation of NS3-NS4B complexes (Scenario 1 in Fig. 1i)
134 but does not disrupt them once formed (Scenario 2). Correspondingly, no reduction of co-captured
135 NS3 was detected when a close analogue of JNJ-A07 (Analogue 2; Extended Data Table 1) was
136 added 48 h after infection (Extended Data Fig. 6c, d) and treatment of cell lysates did not disrupt
137 already established NS3-NS4B complexes (Extended Data Fig. 6e, f).

138 **Unprecedented *in vivo* potency in mice**

139 JNJ-A07 has a very favourable pharmacokinetic profile in mice and rats and no adverse effects
140 were noted in rats up to doses of 300 mg/kg when given for 15 consecutive days via the oral route
141 (Extended Data Table 2a, b). The antiviral effect was next studied in mouse infection models. First,
142 the impact on peak viremia (on day 3 p.i.) in DENV-2 infected ($10^6$ PFU) AG129 mice was studied.
143 Dosing by oral gavage was initiated on the day of infection (starting ~1 hour before infection) and
144 continued twice daily (b.i.d.) until the end of the experiment (Fig. 2a). Viral RNA load in plasma
145 dropped by $3.8\log_{10}$ (30 mg/kg; $P < 0.0001$), $3.6\log_{10}$ (10 mg/kg; $P < 0.0001$), $1.9\log_{10}$ (3 mg/kg;
146 $P < 0.0001$) and $0.8\log_{10}$ (1 mg/kg; $P < 0.05$) copies/ml (Fig. 2b). A dose-dependent and
147 pronounced effect was also observed on viral RNA loads in the spleen, kidney, and liver (Extended
148 Data Fig. 8a-c). Levels of the pro-inflammatory cytokines IL-18, IFN-γ, TNF-α and IL-6 were

149 nearly normalized in plasma of drug-treated infected mice (Extended Data Fig. 7d-g). The effect
150 of JNJ-A07 was next assessed on virus-induced disease and mortality when dosed (oral gavage,
151 b.i.d.) for just 5 consecutive days starting 1 hour before infection (Fig. 2a). AG129 mice (injected
152 on day -1 with an anti-flavivirus antibody to mimic antibody-dependent enhancement[10]) were
153 challenged with $10^6$ PFU DENV-2. Animals were monitored for a maximum period of 25 days. In
154 this model, the survival curve follows a biphasic pattern: early in infection, mice develop a
155 systemic infection leading to vascular leakage, while later, the virus escapes to the brain, resulting
156 in a neurotropic infection and neurological complications. Most (19 out of 20) vehicle-treated mice
157 had to be euthanized between day 4-21 p.i. At a dose of 30 mg/kg, 90% ($P < 0.0001$) survived the
158 infection; at doses of 10, 3 and 1 mg/kg, the survival rate was respectively 80% ($P < 0.0001$), 85%
159 ($P < 0.0001$) and 75% ($P < 0.0001$) (Fig. 2c). Viremia on day 3 p.i. was significantly reduced in
160 all JNJ-A07 dosing groups (Extended Data Fig. 7h). Using the viremia model, we also assessed
161 the efficacy of the NS4B-targeting drug NITD-688[21]. Only mice treated with 100 or 30 mg/kg
162 NITD-688 (b.i.d., oral gavage) had significantly lower viral RNA levels in plasma, respectively
163 $4.3\log_{10}$ and $2.3\log_{10}$ (Extended Data Fig. 7i).

164 The effect of JNJ-A07 was next assessed on the kinetics of DENV-2 replication in AG129 mice
165 following a non-lethal (i.e., $10^2$ PFU) viral challenge (Fig. 2d). In this model, a high peak viral
166 RNA load (~$10^6$ copies/mL) is achieved on day 5-6 p.i. (Fig. 2f, g; for the complete figure, see
167 Extended Data Fig. 8), which is reminiscent of the dynamics during infection in man[22-24]. Mice
168 were treated with 30, 10, 3 or 1 mg/kg JNJ-A07 (orally, b.i.d.) for 6 consecutive days (starting ~1
169 hour before infection). Both treated and vehicle-treated mice exhibited some weight loss (<5%)
170 (Fig. 2e) not attributable to treatment with JNJ-A07. At doses of 30, 10 and 3 mg/kg, average viral
171 RNA levels were mostly at the limit of detection (Fig. 2f, Extended Data Fig. 8c-e). The viral load
172 area under the curve (AUC) for the 30 and 10 mg/kg group was 0% of the vehicle controls and 17%
173 for the 3 mg/kg group. AUC-confidence intervals of the two lowest dosing groups did not differ
174 significantly from the controls as they overlapped with that of the vehicle group.

175 Finally, we explored whether the molecule is sufficiently potent to impact an ongoing, non-lethal
176 ($10^2$ PFU) DENV-2 infection in AG129 mice (mimicking a human therapeutic setting).
177 Administration of JNJ-A07 (30 mg/kg, b.i.d., 6 consecutive days) was initiated either 1 h pre-
178 infection or on subsequent days (Fig. 3a). Initiating treatment on the first 3 days after infection
179 resulted in nearly complete inhibition of viral replication and markedly lower peak viremia

compared to vehicle-treated mice (Fig. 3b-d). When treatment was initiated on day 4 p.i., a time with substantial viremia in the controls, viral loads returned to undetectable levels within 72 hours (Fig. 3e). Even when treatment was first initiated on day 5 or day 6 p.i., the days on which replication reached its peak, an instant antiviral effect was observed (Fig. 3f, g). The impact on the AUC of the viremia was determined from the day treatment was initiated until the end of the experiment. The viral load AUC of JNJ-A07-treated mice was 2% (95% confidence interval [CI]: 0.01-1.42) of the vehicle group (95% CI: 18.57-21.79) when treatment was initiated on day 0. When treatment was initiated on day 1, 2, 3, 4, 5 or 6 p.i., the viral load AUC of JNJ-A07-treated mice was respectively 4% (95% CI: -0.56-3.21), 12% (95% CI: 0.95-6.05), 28% (95% CI: 4.05-12.37), 20% (95% CI: 2.81-7.87), 33% (95% CI: 5.33-10.43), and 52% (95% CI: 6.39-14.76) of that of the vehicle group. Only the AUC-confidence interval of group 8 (treatment start on d6 p.i.) did not differ significantly from group 1 (vehicle, start d0 p.i.) as both intervals overlapped.

## Discussion

There is an urgent need for potent and safe pan-serotype dengue antivirals for the treatment and prophylaxis of infections with dengue virus. Such drugs should lower viral loads during an ongoing infection thereby reducing dengue-associated morbidity and mortality as well as transmission[25-27]. Early diagnostic testing will be key to the employability of prophylactic drugs. Prophylaxis should be beneficial during epidemics for those living in endemic regions and for those traveling to such regions. The concept behind such prophylaxis is that the drug prevents expansion of the inoculum after a mosquito bite. Prophylaxis is for example successfully used in the prevention of malaria[28].

We report on a highly potent, pan-serotype DENV inhibitor targeting NS4B. Drug-resistant variants were only obtained *in vitro* following a lengthy period (up to 40 weeks) of selection, demonstrating a high barrier to resistance. This is explained by the finding that a combination of three mutations in NS4B is required to reach high-level resistance. This characteristic makes it rather unlikely that drug-resistant variants will readily emerge in drug-treated patients. Moreover and remarkably, the mutations in NS4B appear to render the resistant variants unable to replicate in mosquito cells. This suggests that even if such mutants would develop, they may not be transmitted from human to human via the insect vector.

Resistance selection and reverse genetics studies pinpoint NS4B as the molecular target of JNJ-A07. NS4B is a multi-transmembrane protein residing in the endoplasmic reticulum membrane as

210 part of the DENV replication complex. It forms a complex with NS3, which is essential for viral
211 replication[20,29]. Several functions have been ascribed to NS4B[30-32]. *In vitro* studies revealed that
212 NS4B dissociates NS3 from single-stranded RNA and enhances NS3 helicase activity[33]. No
213 enzymatic activity has been shown to be associated with NS4B. We here demonstrate that JNJ-
214 A07 blocks *de novo* formation of the NS3-NS4B complex; established complexes appear relatively
215 resistant to the compound. JNJ-A07 prevents the formation of the NS3-NS4B complex but does
216 this inefficiently when NS4B carries mutations associated with drug-resistance. In fact, a striking
217 correlation was observed between drug-resistance in a DENV replication assay on the one hand
218 and the insensitivity of the interaction between NS3 and NS4B mutants on the other. This provides
219 compelling evidence that JNJ-A07 interferes with NS3-NS4B complex formation. Interestingly,
220 L94F (the mutation conferring the highest level of resistance but resulting in increased replication
221 fitness) has been reported as a pseudo-reversion compensating the replication defect caused by the
222 M142A mutation in NS4B[20]. As is the case for Q134A, M142A resides in the cytosolic loop of
223 NS4B and impairs the NS3-NS4B interaction, thereby largely reducing viral replication. Our
224 findings suggest that JNJ-A07 blocks the NS3-NS4B interaction by inducing a conformational
225 change of the cytosolic loop. In addition, the observed accumulation of the NS4A-2K-NS4B
226 precursor suggests that JNJ-A07 slows down the cleavage kinetics of the precursor (e.g., by
227 binding to the NS4B moiety and altering precursor folding or accessibility of the cleavage site).

228 JNJ-A07 has a very favourable pharmacokinetic and safety profile in mice and rats and exerts
229 unprecedented potency in DENV-2 mouse infection models. It is highly effective in reducing viral
230 loads (even at low doses to levels below the LOD) and virus-induced disease. Importantly, even
231 when start of treatment was delayed for several days after infection, a rapid and marked reduction
232 in viral load was observed. JNJ-A07 or close analogues with comparable safety, pharmacokinetics
233 and potency may have the potential to be effective in both prophylactic and therapeutic settings
234 against DENV infections in man. Recently, NITD-688 was reported as a NS4B-targeting drug, yet
235 with an unknown mechanism[21]. The resistance mutation profile differs from that of JNJ-A07,
236 indicative of a different mode of action. JNJ-A07 is profoundly more efficacious than NITD-688
237 in DENV-2 mouse infection models, both in a prophylactic and a therapeutic setting.

238 In conclusion, we demonstrate for the first time that blocking the interaction between two viral
239 proteins (NS3 and NS4B) results in pronounced antiviral activity. The NS3-NS4B interaction
240 represents an excellent target for the development of pan-serotype DENV inhibitors with a high

241 barrier to resistance. The unprecedented potency warrants further development of this class of
242 compounds.

243

244 **References**


245 1. World Health Organization. Dengue and severe dengue. Factsheet. WHO, Geneva,
246 Switzerland. https://www.who.int/news-room/fact-sheets/detail/dengue-and-severe-dengue
247 (15 April 2019).

248 2. Bhatt, S. *et al.* The global distribution and burden of dengue. *Nature* **496**, 504-507 (2013).

249 3. Ayukekbong, J. A., Oyero, O. G., Nnukwu, S. E., Mesumbe, H. N. & Fobisong, C. N. Value
250 of routine dengue diagnosis in endemic countries. *World J. Virol.* **6**, 9-16 (2017).

251 4. Paixão, E. S., Teixeira, M. G. & Rodrigues, L. C. Zika, chikungunya and dengue: the causes
252 and threats of new and re-emerging arboviral diseases. *BMJ Glob. Health* **3**, e000530 (2018).

253 5. Simmons, C. P., Farrar, J. J., Nguyen, vV. & Wills, B. Dengue. *N. Engl. J. Med.* **366**, 1423-
254 1432 (2012).

255 6. Messina, J. P. *et al*. The current and future global distribution and population at risk of dengue.
256 *Nat. Microbiol.* **4**, 1508-1515 (2019).

257 7. Duong, V. *et al.* Asymptomatic humans transmit dengue virus to mosquitoes. *Proc. Natl.*
258 *Acad. Sci. U S A* **112**, 14688–14693 (2015).

259 8. ten Bosch, Q. A. *et al*. Contributions from the silent majority dominate dengue virus
260 transmission. *PLoS Pathog.* **14**, e1006965 (2018).

261 9. Halstead, S. B. Pathogenesis of Dengue: Dawn of a New Era. *F1000Res.* **4** (F1000 Faculty
262 Rev), 1353 (2015).

263 10. Katzelnick, L. C. *et al.* Antibody-dependent enhancement of severe dengue disease in humans.
264 *Science* **358**, 929-932 (2017).

265 11. WHO. Dengue vaccine: WHO position paper – July 2016. *Wkly Epidemiol. Rec.* **91**, 349-64
266 (2016).

267 12. Wilder-Smith, A. et al. Deliberations of the strategic advisory group of experts on
268 immunization on the use of CYD-TDV dengue vaccine. *Lancet Infect. Dis.* **19**, e31–38 (2019).

269 13. WHO. Dengue vaccine: WHO position paper – September 2018. *Wkly Epidemiol. Rec.* **93**,
270 457–476 (2018).

271 14. Low, J. G., Gatsinga, R., Vasudevan, S. G. & Sampath, A. Dengue Antiviral Development: A
272 Continuing Journey. In *Dengue and Zika: Control and Antiviral Treatment Strategies.*
273 *Advances in Experimental Medicine and Biology* 319-332 (Vol 1062, Springer, Singapore,
274 2018).

275 15. Whitehorn, J. *et al.* Dengue therapeutics, chemoprophylaxis, and allied tools: state of the art
276 and future directions. *PLoS Negl. Trop. Dis.* **8**, e3025 (2014).

277 16. Bardiot, D. *et al.* Discovery of Indole Derivatives as Novel and Potent Dengue Virus
278 Inhibitors. *J. Med. Chem.* **61**, 8390-8401 (2018).

279 17. Schmid, M. A. & Harris, E. Monocyte recruitment to the dermis and differentiation to
280 dendritic cells increases the targets for dengue virus replication. *PLoS Pathog.* **10**, e1004541
281 (2014).

282 18. Touret, F. *et al.* Phylogenetically based establishment of a dengue virus panel, representing
283 all available genotypes, as a tool in dengue drug. *Antiviral Res.* **168**, 109-113 (2019).

284 19. Płaszczyca, A. *et al*. A novel interaction between dengue virus nonstructural protein 1 and the
285 NS4A-2K-4B precursor is required for viral RNA replication but not for formation of the
286 membranous replication organelle. *PLoS Pathog.* **15**, e10077362019 (2019).

287 20. Chatel-Chaix, L. *et al.* A combined genetic-proteomic approach identifies residues within
288 dengue virus NS4B critical for interaction with NS3 and viral replication. *J. Virol.* **89**, 7170-
289 7186 (2015).

290 21. Moquin, S. A. *et al*. NITD-688, a pan-serotype inhibitor of the dengue virus NS4B protein,
291 shows favorable pharmacokinetics and efficacy in preclinical animal models. *Sci. Transl.*
292 *Med.* **13**, eabb2181 (2021).

293 22. Clapham, H. E., Tricou, V., Van Vinh Chau, N., Simmons, C. P. & Ferguson, N. M. Within-
294 host viral dynamics of dengue serotype 1 infection. *J. R. Soc. Interface* **11**, 20140094 (2014).

295 23. Sim, S. *et al*. Tracking Dengue Virus Intra-host Genetic Diversity during Human-to-Mosquito
296 Transmission. *PLoS Negl. Trop. Dis.* **9**, e0004052 (2015).

297 24. Simmons, C. P. *et al*. Recent advances in dengue pathogenesis and clinical management.
298 *Vaccine* **33**, 7061-7068 (2015).

299 25. Nguyen, N. M. *et al*. Host and viral features of human dengue cases shape the population of
300 infected and infectious Aedes aegypti mosquitoes. *Proc. Natl. Acad. Sci.* **110**, 9072–9077
301 (2013).

302 26. Simmons, C. P. *et al*. Therapeutics for dengue: recommendations for design and conduct of
303 early-phase clinical trials. *PLoS Negl. Trop. Dis.* **6**, e1752 (2012).

304 27. WHO. Unlocking the potential of preventive therapies for malaria. WHO, Geneva,
305 Switzerland. https://www.who.int/malaria/media/preventive-therapies/en/ (7 April 2017).

306 28. Low, J. G., Ooi, E. E. & Vasudevan, S. G. Current Status of Dengue Therapeutics Research
307 and Development. *J. Infect. Dis.* **215**, S96-S102 (2017).

308 29. Zou, J. *et al*. Characterization of dengue virus NS4A and NS4B protein interaction. *J Virol.*
309 **89**, 3455-3470 (2015).

310 30. Miller, S., Sparacio, S. & Bartenschlager, R. Subcellular localization and membrane topology
311 of the Dengue virus type 2 Non-structural protein 4B. *J. Biol. Chem.* **281**, 8854-8863 (2006).

312 31. Chatel-Chaix, L. *et al.* Dengue Virus Perturbs Mitochondrial Morphodynamics to Dampen
313 Innate Immune Responses. *Cell Host Microbe* **20**, 342-356 (2016).

314 32. Zmurko, J., Neyts, J. & Dallmeier, K. Flaviviral NS4B, chameleon and jack-in-the-box roles
315 in viral replication and pathogenesis, and a molecular target for antiviral intervention. *Rev.*
316 *Med. Virol.* **25**, 205-223 (2015).

317 33. Umareddy, I., Chao, A., Sampath, A., Gu, F. & Vasudevan, S. G. Dengue virus NS4B
318 interacts with NS3 and dissociates it from single-stranded RNA. *J. Gen. Virol.* **87**, 2605-2614
319 (2006).

320

321

| Cell type | DENV-2 strain | Antiviral activity | | Toxicity | |
|---|---|---|---|---|---|
| | | $EC_{50}$ (µM) | $EC_{90}$ (µM) | $CC_{50}$ (µM) | SI* |
| Vero | 16681 | 0.0001 ± 0.00007 | 0.0005 ± 0.0004 | 13 ± 1.1 | 130,000 |
| Huh-7 | 16681 | 0.0008 ± 0.0002 | 0.002 ± 0.001 | >25 | >31,000 |
| THP-1/DC-SIGN | 16681 | 0.0007 ± 0.0002 | 0.001 ± 0.0005 | >0.5 | >714 |
| ImDCs | 16681 | 0.002 ± 0.001 | 0.009 ± 0.005 | 140 ± 62 | 70,000 |
| C6/36 | RL | 0.003 ± 0.0006 | 0.007 ± 0.004 | 18 ± 4.5 | 6,000 |
| Vero | RL | 0.0002 ± 0.00004 | 0.0005 ± 0.00003 | 14 ± 0.3 | 70,000 |

| Serotype | Genotype | Strain | $EC_{50}$ (µM) | $EC_{90}$ (µM) |
|---|---|---|---|---|
| DENV-1 | G1 | Djibouti | <0.00006 ± 0.00004 | <0.0001 ± 0.0001 |
| DENV-1 | G3 | Malaysia†‡ | 0.0003 ± 0.00007 | 0.0007 ± 0.0001 |
| DENV-1 | G4 | Indonesia | <0.00008 ± 0.00005 | <0.0002 ± 0.0002 |
| DENV-1 | G5 | France - Toulon | <0.00003 ± 0.00001 | <0.0002 ± 0.0002 |
| DENV-2 | Asian America | Martinique‡ | 0.004 ± 0.005 | 0.005 ± 0.005 |
| DENV-2 | American | Trinidad | <0.00003 ± 0.000009 | <0.00007 ± 0.00007 |
| DENV-2 | Cosmopolitan | France - Toulon | <0.00007 ± 0.00005 | <0.0002 ± 0.0002 |
| DENV-2 | Asian I | Thailand‡ | 0.001 ± 0.0002 | 0.001 ± 0.000002 |
| DENV-2 | Asian II | Papua New Guinea† | <0.00004 ± 0 | <0.00007 ± 0.00004 |
| DENV-2 | Sylvatic | Malaysia† | <0.00006 ± 0.00003 | 0.0002 ± 0.00008 |
| DENV-3 | G1 | Malaysia | 0.0005 ± 0.0002 | 0.001 ± 0.0003 |
| DENV-3 | G2 | Thailand | 0.001 ± 0.0007 | 0.002 ± 0.0002 |
| DENV-3 | G3 | Bolivia | 0.0004 ± 0.0003 | 0.002 ± 0.0009 |
| DENV-3 | G5 | H87‡ | 0.001 ± 0.0005 | 0.002 ± 0.0007 |
| DENV-3 | G5 | Brazil†§ | 0.0002 ± 0.0002 | 0.0006 ± 0.0005 |
| DENV-4 | G1 | India | <0.00004 ± 0 | <0.0001 ± 0.0001 |
| DENV-4 | G2a | Malaysia | 0.003 ± 0.003 | 0.004 ± 0.004 |
| DENV-4 | G2b | Martinique | <0.0001 ± 0.0001 | 0.001 ± 0.0003 |
| DENV-4 | G2b | Brazil | <0.0002 ± 0.0001 | 0.0006 ± 0.0001 |
| DENV-4 | G3 | Thailand† | 0.006 ± 0.006 | 0.01 ± 0.002 |
| DENV-4 | Sylvatic | Malaysia† | 0.0003 ± 0.00002 | 0.0009 ± 0.0004 |

322

323 **Legends to figures**

324 **Table 1 Antiviral activity of JNJ-A07 against DENV serotypes.**

325 *Selectivity index (SI): Ratio $CC_{50}$ / $EC_{50}$.

326 †DENV strain generated using infectious subgenomic amplicons (ISA).

327 ‡DENV strain carrying the T108I mutation in NS4B.

328 §DENV strain containing the T108A mutation in NS4B.

329 Antiviral assays were carried out on Vero E6 cells. Antiviral data for DENV-2 represent average
330 values ± s.d. from two (Vero and C6/36 cells infected with DENV-2 RL, and imDCs infected with
331 DENV-2/16681), three (THP-1/DC-SIGN cells infected with DENV-2/16681), or at least five
332 (Vero and Huh-7 cells infected with DENV-2/16681) independent experiments. Antiviral data for
333 other serotypes represent average values ± s.d. from at least two independently performed
334 experiments ($n$ = 2 to 6). DENV serotype panel was selected as reported previously[18]. $CC_{50}$, 50%
335 cytotoxic concentration; $EC_{50}$, 50% effective concentration; $EC_{90}$, 90% effective concentration;
336 ImDCs, immature dendritic cells.

337 **Fig. 1 Identification of molecular target of JNJ-A07. a**, Molecular structure of JNJ-A07. **b**,
338 Schematic of membrane topology of DENV NS4B[30,32]. JNJ-A07-selected resistance mutations in
339 orange were present in 100% of the quasispecies at endpoint (P43) in one of the two independently
340 selected resistant strains (sample A and B). Resistance mutations in black were present in <100%
341 of the quasispecies at endpoint; mutations in blue appeared and disappeared. **c**, Mutations present
342 in 100% of the quasispecies at endpoint in sample A and/or B. Dark grey bars represent mutations
343 present at P15; light grey bars mutations present at P43. 'A' and 'B' refer to A and B sample,
344 respectively. **d**, Effect of resistance mutations on replication fitness. **e**, Level of compound
345 resistance imposed by NS4B resistance mutations. **f**, Representative Western blot. The full,
346 representative Western blot is depicted in Extended Data Fig. 5b. For the uncropped Western blot
347 images, see Supplementary Fig. 1. **g**, Impact of JNJ-A07 on interaction between NS3 and WT or
348 mutant NS4B. For each sample, the ratio of NS3 over all NS4B species was normalized to the
349 average untreated WT ratio. **h**, Impact of JNJ-A07 on forming or pre-formed NS3-NS4B protein
350 complexes. JNJ-A07-mediated treatment effect on the indicated ratios was assessed using linear
351 mixed effects models. A random effect for each replicate was included. Models were fitted for the

352 three ratios separately. Sidak's multiplicity correction was applied to the intervals to account for
353 multiple testing. **i**, Model on the mode-of-action, suggesting that JNJ-A07 blocks *de novo*
354 formation of NS3-NS4B complexes (Scenario 1) but does not disrupt existing ones (Scenario 2).
355 Data are average ± s.d. (bars in **d**, **e**) or estimated marginal means per mutation and treatment with
356 their 95% CI (**g**, **h**) from three (**h**) or at least three (**d**, **e**, **g**) independent experiments.

357 **Fig. 2 *In vivo* efficacy of JNJ-A07 on viremia and survival in a prophylactic setting. a**,
358 Schematic outline of viremia and survival studies using AG129 mice. **b**, **c**, Effect of JNJ-A07 on
359 viremia on day 3 p.i. (**b**) and on survival (**c**) in mice treated twice-daily with 30 (white), 10 (light
360 blue), 3 (dark blue) or 1 (grey) mg/kg JNJ-A07, compared to vehicle-treated mice (red). Treatment
361 started 1 hour before infection. In the survival study, mice received an Anti-Flavivirus antibody
362 one day before infection. Data are from two independent studies with $n = 8$ (viremia) or $n = 10$
363 (survival) per group. **d**, Schematic outline of the *in vivo* kinetics study. Each treatment group was
364 sub-divided in group A and B ($n = 8$, each) for blood collection on alternating days. **e**, Weight
365 curves (average values ± s.d.) of AG129 mice in the different treatment groups. Colors of the dots
366 represent the different dosing groups ($n = 8$, each), as specified in (**b**); green dots represent the 0.3
367 mg/kg dosing group. **f-g**, Inhibitory effect of JNJ-A07 on viremia in mice treated twice-daily with
368 10 mg/kg ($n = 8$) or 1 mg/kg ($n = 8$), as compared to vehicle-treated mice ($n = 16$). For the complete
369 figure, see Extended Data Fig. 8. Treatment started 1 hour before infection. Data (median ± s.d.)
370 are from two independent studies. Undetermined Ct values were imputed at a Ct value of 40
371 (=LOD), corresponding to $2.6\log_{10}$ viral RNA copies/mL. For two-sided statistical analysis the
372 Kruskal-Wallis test (viremia) or the Fisher's exact test (survival) was used. *P* values were adjusted
373 using the Holm's multiple comparisons correction method. The mean AUC value and 95% CI was
374 determined for (**f-g**). In case CIs did not overlap, groups were considered to differ significantly.
375 LLOQ, lowest level of quantification; HEP, humane endpoints.

376 **Fig. 3 *In vivo* efficacy of JNJ-A07 on kinetics of DENV replication in a therapeutic setting. a**,
377 Schematic outline of the *in vivo* kinetic studies whereby treatment was started on various days
378 after DENV-2 challenge (groups 3-8), while in the control groups (vehicle and JNJ-A07) treatment
379 was started on the day of infection (groups 1 and 2, respectively). Each treatment group ($n = 8$,
380 each) was sub-divided in group A and B ($n = 4$, each) for blood collection on alternating days. **b-**
381 **g**, Inhibitory effect of JNJ-A07 on viremia with the start of treatment at various time points p.i. in
382 AG129 mice treated twice-daily with 30 mg/kg for 6 consecutive days. In the delayed treatment

383 groups (group 3-8), treatment with JNJ-A07 was started on day 1 (green dots/bar), day 2 (grey
384 dots/bar), day 3 (black dots/bar), day 4 (light blue dots/bar), day 5 (yellow dots/bar), or day 6 (dark
385 blue dots/bar) p.i. As controls, two groups of mice received treatment on the day of infection:
386 group 1 (vehicle; red dots/bar) and group 2 (JNJ-A07; white dots/bar). Data (median ± s.d.) are
387 from a single experiment. Undetermined Ct values were imputed at a Ct value of 40 (=LOD),
388 corresponding to 2.6$\log_{10}$ viral RNA copies/mL. The mean AUC value and 95% CI was
389 determined for each group. In case CIs did not overlap, groups were considered to differ
390 significantly. LLOQ, lowest level of quantification.

391 **METHODS**

392 **Compounds**

393 The synthesis of early chemical analogues of JNJ-A07 and derivatives is reported elsewhere[16]. The
394 synthesis of Analogue 1 is described in WO2016/050841 (Compound 1A) and that of Analogue 2
395 in WO2016/050831 (Compound 1A). The synthesis of JNJ-A07 is published in WO2017/167951
396 (example 4B). The synthesis and chemical characterization of Analogue 1, Analogue 2 and JNJ-
397 A07 is also is provided as Supplementary Information to this paper (Supplementary Methods). For
398 *in vitro* experiments, compounds were dissolved in 100% DMSO as a 10 mg/mL or a 5 mM stock.
399 The nucleoside analogue 7-deaza-2'-*C*-methyladenosine (7DMA; CAS No 443642-29-3) was
400 purchased from Carbosynth (Berkshire, UK). The synthesis of the DENV NS4B inhibitor NTID-
401 688 was carried out in-house following a synthetic route as described in the literature[21] and in
402 patent WO 2019/244047 A1.

403 **Cells**

404 Vero cells (African green monkey kidney cells; ECACC: CL 84113001) were maintained in
405 Eagle's minimum essential medium (MEM) supplemented with 10% fetal bovine serum (FBS)
406 (Sigma-Aldrich, St. Louis, Mo), 2 mM L-glutamine and 0.02 mg/mL gentamicin (Thermo Fisher
407 Scientific, Waltham, MA). Vero E6 cells (ATCC: CRL-1586) were cultured in MEM
408 supplemented with 7.5% heat-inactivated FBS, 2 mM L glutamine, and 100 units/mL penicillin-
409 streptomycin (Sigma). In the antiviral experiments with Vero E6 cells, 2.5% heat-inactivated FBS
410 was used. Huh-7 hepatoma-derived cells were maintained in Dulbecco's modified Eagle's medium
411 (DMEM), supplemented with 10% FBS, 2 mM L-glutamine and 0.02 mg/mL gentamicin. In
412 antiviral assays using Vero and Huh-7 cells, the culture media contained 2% FBS instead of 10%

413 FBS. Huh-7 replicon cells were cultured in the same medium as mentioned above, supplemented
414 with 75 µg/mL hygromycin B (Roche Applied Science, Penzberg, Germany). Huh-7 cells stably
415 expressing the T7 polymerase and the DENV protease complex NS2B-NS3 (Huh7-T7/NS2B-NS3
416 cells) were generated by lentiviral transduction, as described previously[20]. Cells were cultured at
417 37 °C and 5% $CO_2$ in DMEM, supplemented with 10% FBS, 2 mM L-glutamine, 100 U/mL
418 penicillin, 100 µg/mL streptomycin, 5 µg/ml zeocin, 1 µg/mL puromycin and nonessential amino
419 acids. Antiviral assays were performed using DMEM/2% FBS. THP-1 Dendritic Cell-Specific
420 Intercellular adhesion molecule-3-Grabbing Non-integrin (DC-SIGN) cells (TIB-202; ATCC)
421 were propagated in RPMI (Lonza) supplemented with 10 % heat-inactivated FBS (F7524; Sigma-
422 Aldrich) and 0.04 % gentamicin (Gibco-Life Technologies). C6/36 mosquito cells (from *Aedes*
423 *albopictus*; ATCC CCL-1660) were cultivated in the absence of 5% $CO_2$ at 28 °C in Leibovitz's
424 L-15 medium (Thermo Fisher Scientific), supplemented with 10% FBS, 1% non-essential amino
425 acids (Thermo Fisher Scientific), 1% HEPES buffer (Thermo Fisher Scientific), and 1% penicillin
426 (100 U/mL)/streptomycin (100 µg/mL) solution (Thermo Fisher Scientific). Human peripheral
427 blood mononuclear cells (PBMCs) were prepared from fresh buffy coats (obtained 24 hours before
428 preparation from the Belgian Red Cross) of healthy donors using a standard Ficoll centrifugation
429 protocol. Monocytes were isolated from the PBMC population with Miltenyi cluster of
430 differentiation (CD)14 beads (Miltenyi Biotec, Bergisch Gladbach, Germany). Monocytes were
431 differentiated to imDCs using interleukin-4 (IL-4, R&D Systems) and granulocyte-macrophage
432 colony-stimulating factor (GM-CSF, R&D Systems). Multiple donors were used to account for
433 potential variation in responses due to varying representation of genetic and societal backgrounds.
434 Cells were cultured at 37 °C and 5% $CO_2$ unless stated otherwise. All cell lines (Vero, Huh-7,
435 THP-1/DC-SIGN and C6/36) were regularly tested for mycoplasma contamination.

436 **Viruses**

437 Lab-adapted strain DENV-2/16681 was produced by transfection of *in vitro* transcribed RNA of
438 plasmid pFK-DVs into Huh-7 cells. This plasmid encodes for the full-length DENV-2/16681.
439 Plasmid pFK-DVs was obtained by insertion of a synthetic copy of the full-length genomic
440 sequence of DENV-2 Strain 16681 (Genbank Accession NC_001474) into the low-copy plasmid
441 vector pFK[34]. Moreover, the parental vector pFK was modified by insertion of the SP6 promoter
442 upstream of the DENV 5' nontranslated region (5'NTR) to enable synthesis of authentic viral RNA
443 by *in vitro* transcription. This plasmid was licensed from Prof. R. Bartenschlager.

444 DENV-2/16681/eGFP, carrying eGFP N terminally of the capsid, was produced by the transfection
445 of *in vitro* transcribed RNA of plasmid pFK-DV-G2A into Huh-7 cells[34]. This plasmid encodes
446 for eGFP and the full-length DENV-2/16681. The infectious cDNA clone pFK-DVs served as
447 parental construct for cloning of the dengue reporter virus construct DENV-G2A. The reporter
448 gene is followed by the 2A peptide of Thosea asigna virus to liberate the eGFP from the DENV
449 polyprotein during/after translation. This plasmid was licensed from Prof. R. Bartenschlager. The
450 resulting recombinant virus is referred to as DENV-2/16681/eGFP.

451 Four DENV-1 strains were used: Djibouti (D1/H/IMTSSA/98/606), Genotype 1, Accession
452 Number GenBank AF298808; Malaysia, produced by Infectious Subgenomic Amplicons (ISA)[35],
453 Genotype 3, Accession Number GenBank EF457905.1; Indonesia (JKT 1186 TVP 949),
454 Genotype 4, Accession Number GenBank EUO7031; and France-Toulon (CNR 25329),
455 Genotype 5, Accession Number GenBank MF004384, obtained from the European Virus Archive
456 (EVA).

457 Six DENV-2 strains were used: Martinique (H/IMTSSA-MART/98-703), Asian America,
458 Accession Number GenBank AF208496; Trinidad (1751 TC 544), American, Accession Number
459 GenBank EU073981.1, EVA; France-Toulon (CNR 25679), Cosmopolitan, Accession Number
460 GenBank MF004385, EVA; Thailand (CNR 25326), Asian I, EVA; Papua New Guinea (ISA),
461 Accession Number GenBank FJ906959.1, Asian II; and Malaysia (ISA), Accession Number
462 GenBank FJ467493.1, Genotype Sylvatic.

463 Five DENV-3 strains were used: Malaysia (CNR 17046), Genotype 1, Accession Number
464 GenBank MF004386, EVA; Thailand (CNR 15418), Genotype 2, Accession Number GenBank
465 MH888332, EVA; Bolivia (Strain 4025), Genotype 3, Accession Number GenBank MH888333,
466 EVA; H87, Genotype 5, Accession Number GenBank M93130; and Brazil (ISA), Genotype 5,
467 Accession Number GenBank JN697379.1.

468 Six DENV-4 strains were used: India (strain G11337), Genotype 1, Accession Number GenBank
469 JF262783.1**;** Malaysia (CNR 16861), Genotype 2a, Accession Number GenBank MH888334,
470 EVA; Martinique (Strain 017), Genotype 2b, EVA; Brazil (BeH 403714), Genotype 2b, Accession
471 Number GenBank JQ513345.1; Thailand (ISA), Accession Number GenBank AY618988.1,
472 Genotype 3; and Malaysia, Accession Number GenBank JF262779.1, Genotype Sylvatic.

473 DENV-1 Genotype 2 and DENV-3 Genotype 4 are currently not available as full sequences in
474 public databases such as the National Center for Biotechnology Information or Virus Pathogen
475 Resource (ViPR; www.viprbrc.org).

476 Four non-DENV flaviviruses were used: Zika virus (ZIKV; H/PF/2013, French Polynesia,
477 GenBank KJ776791), Japanese encephalitis virus (JEV; CNS769-Laos 2009, Laos, GenBank
478 KC196115), West Nile virus (WNV; R94224, CDC Human Brain 29-09-2008, Wisconsin,
479 GenBank MF004388) and yellow fever virus (YFV; 88-99, Bolivia, GenBank MF004382).

480 In antiviral assay using Vero cells and C6/36 mosquito cells, time-of-drug-addition experiments,
481 *in vitro* resistance selection experiments, and *in vivo* efficacy studies, the DENV-2 Rega Labstrain
482 -referred to as 'DENV-2 RL'- was used, Accession Number GenBank MW741553. This strain is
483 kindly provided by Dr. V. Deubel, formerly at the Institute Pasteur, Paris. For *in vivo* studies, high-
484 titer stocks were generated by propagating in C6/36 mosquito cells and subsequently concentrating
485 either by ultracentrifugation or tangential flow filtration using tangential flow filtration capsules
486 (Minimate TFF; Pall Life Sciences, Dreieich, Germany), according to the manufacturer's protocol.
487 Infectious virus titers (plaque forming units per mL; PFU/mL) were determined by performing
488 plaque assays on baby hamster kidney (BHK) cells, as described previously[36].

489 **DENV-2/16681 antiviral assays**

490 The antiviral activity of JNJ-A07 was determined against DENV-2/16681/eGFP in a phenotypic
491 antiviral assay with enhanced green fluorescent protein (eGFP) readout, a measure for the amount
492 of virus. The assay was performed on three different cell types (Vero, Huh-7 and THP-1/DC-
493 SIGN) to exclude cell-specific activity of the compound. In brief, $2.5 \times 10^3$ Vero cells or Huh-7
494 cells or $7.5 \times 10^3$ THP-1/DC-SIGN cells were seeded in 384-well plates containing 9-fold serially
495 diluted test compound. After incubating for 24 hours at 37 °C, Vero and Huh-7 cells were infected
496 with DENV-2/16681/eGFP at a multiplicity of infection (MOI) of 1 and 5, respectively. THP-
497 1/DC-SIGN cells were infected immediately after seeding of the cells with DENV-2/16681/eGFP
498 at a MOI of 0.5. After 3 days of incubation at 37 °C, viral replication was quantified by measuring
499 eGFP expression in the cells with a laser microscope. Following eGFP readout, the cytotoxic effect
500 of JNJ-A07 was evaluated using the ATPlite cell viability luminescence assay (PerkinElmer,
501 Waltham, MA), according to the supplier's instructions.

502 In antiviral assays with imDCs, DENV-2/16681 was used, followed by detection of DENV
503 antigens using flow cytometry. Monocytes, isolated from PBMCs, were counted and $3 \times 10^5$ cells
504 were seeded in wells of a 96-well plate. Next, monocytes were differentiated into imDCs by
505 incubating them for 5 days at 37°C in the presence of 20 ng/mL IL-4 and GM-CSF. The medium
506 was then discarded and imDCs were infected with DENV-2/16681 at an MOI of 0.5 in the presence
507 or absence of JNJ-A07. On day 2 p.i., cells were permeabilized and fixed with Cytofix/Cytoperm
508 buffer (BD Biosciences) and stained with primary anti-prM antibody (Anti-Dengue Virus
509 Complex Antibody, clone D3-2H2-9-21; MAB8705, 1:400 diluted; Merck), followed by
510 secondary goat anti-mouse AlexaFluor488 antibody (A-10680, 1:500 diluted; Life
511 Technologies/ThermoFisher Scientific). The percentage of cells expressing prM (7-11% for
512 untreated virus control samples) was quantified by fluorescence-activated cell sorting (FACS) on
513 a CANTO II apparatus (BD Biosciences, Franklin Lakes, NJ). Toxicity of JNJ-A07 was assessed
514 with FACS in non-infected imDCs by measuring the viability dye eFluor 660 (ThermoFisher
515 Scientific) added to the cells prior to their fixation.

516 **Antiviral assays using DENV-2 RL strain on Vero and C6/36 cells**

517 Virus yield reduction assays on Vero cells were performed essentially as described previously[16].
518 In short, Vero cells were seeded at a density of $4 \times 10^4$ cells/well in 100 µL DMEM/10%FBS
519 medium in 96-well plates. Next day, cells were infected with DENV-2 RL strain (MOI = 0.01),
520 diluted in MEM/2%FBS assay medium (100 µL/well). Cells were incubated for 2 hours, after
521 which the viral inoculum was removed. After rinsing the cells three times with assay medium, 5-
522 fold serial dilutions (concentration ranged from 50 – 0.0001 µg/mL in screening assays and from
523 1 – 0.000003 µg/mL in 'confirmation-of-antiviral-activity' assays) of the test compounds were
524 added to the cells. After an incubation period of 4 days, supernatant was harvested and the viral
525 RNA load was determined by RT-qPCR, as described previously[37]. A potential toxic effect on host
526 cells was tested in parallel using the same protocol. In toxicity assays, virus infection was omitted
527 and the serial dilution of compounds was started at a higher concentration (concentration ranged
528 from 400 – 0.001 µg/mL; only in 'confirmation-of-antiviral-activity' assays). After 4 days of
529 incubation, colorimetric readout was performed using the MTS/PMS method (Promega, Leiden,
530 The Netherlands), as described previously[38].

531 In antiviral assays using C6/36 mosquito cells, cells were seeded at a density of $2.5 \times 10^5$ cells/well
532 in 100 µL culture medium (also see 'Cells' section) in 24-well plates. Next day, culture medium
533 was replaced by 100 µL/well assay medium (in assay medium 10% FBS is replaced by 2% FBS)
534 containing 2-fold serial dilutions (concentration ranged from 50 – 0.002 µg/mL) of the test
535 compounds. DENV-2 RL strain (MOI = 0.02; 100 µL/well), diluted in assay medium, was added
536 to the cells. After a 7-day incubation period at 28 °C, supernatant was harvested and the viral RNA
537 load was determined by RT-qPCR, as described for the Vero cells. A potential toxic effect on host
538 cells was tested in parallel using the same protocol. However, virus infection was omitted and the
539 2-fold serial dilution of compounds ranged from 50 – 0.4 µg/mL. On day 7 p.i., cells were fixed
540 with 2% paraformaldehyde in PBS. Cell nuclei were stained using DAPI (4',6-diamidino-2-
541 fenylindool; Thermo Fisher Scientific) and readout was performed using an ArrayScan XTI High
542 Content Analysis Reader (Thermo Fisher Scientific). The 50% effective concentration (the
543 compound concentration that is required to inhibit viral RNA replication by 50%; $EC_{50}$) and the
544 50% cytotoxic concentration (the concentration that reduces the total cell number by 50%; $CC_{50}$)
545 was determined using logarithmic interpolation.

546 **Antiviral activity against clinical isolates covering four DENV serotypes**

547 One day prior to infection, $5 \times 10^4$ Vero E6 cells were seeded in 100 µL assay medium (containing
548 2.5% FBS) in 96-well plates. Next day, eight 2- or 3-fold serial dilutions of JNJ-A07 (for DENV:
549 100 – 0.04 nM; for other flaviviruses: 5 – 0.02 µM; final concentration), in triplicates or duplicates
550 (for control), were added to the cells (25 µL/well). Four virus control wells (per virus) were
551 supplemented with 25 µL medium and four cell control wells were supplemented with 50 µL of
552 medium. After 15 minutes, 25 µL of a virus dilution was added to the wells at an MOI that was
553 determined such that the viral growth reached its peak or the beginning of the plateau on day 4 p.i.
554 Plates were incubated at 37 °C for 4 days (DENV and ZIKV), 3 days (JEV) 2.5 days (YFV), or
555 2 days (WNV). After incubation, 100 µL of the supernatant was collected for viral RNA isolation.

556 **Time-of-drug-addition assay**

557 Vero cells were seeded at a density of $2 \times 10^5$ cells/well in a 24-well plate and the following day
558 infected with DENV-2 RL strain (MOI = 1) in assay medium. JNJ-A07 (at a concentration of 10×
559 $EC_{50}$, as determined in the antiviral assay) was added at either the time point of virus infection or
560 at 4, 10, 12, 14, 16, 18, and 22 hours p.i. At 24 hours p.i., intracellular RNA was isolated using the

561 RNeasy minikit (Qiagen) and DENV RNA levels were quantified by RT-qPCR. In parallel
562 experiments, 7DMA (14 µM) was used as a reference compound. To monitor intracellular viral
563 RNA production (i.e., viral kinetics) during one replication cycle in untreated cells, confluent Vero
564 cells in a 24-well plate ($2 \times 10^5$ cells/well) were infected and incubated for 1 hour. After removing
565 the inoculum and washing the cells, assay medium was added, and cells were harvested at similar
566 time points as indicated for the time-of-drug-addition assay. Viral RNA replication was monitored
567 by means of RT-qPCR.

568 **RNA isolation and quantitative RT-qPCR**

569 Supernatant was transferred to 96 well S-Bloc from Qiagen (Venlo, The Netherlands), preloaded
570 with buffer VXL and extracted by the Cador Pathogen 96 QIAcube HT kit run on QIAcube HT
571 automat (Qiagen), as described by the manufacturer. For DENV, purified RNA was eluted in 80
572 µL of AVE buffer (Qiagen); for the other flaviviruses, purified RNA was eluted in water.

573 DENV RNA was quantified by real-time RT-qPCR using 3.8 µL of RNA and 6.2 µL of RT-qPCR
574 mix (GoTaq Probe one-step RT-qPCR system, Promega, Fitchburg, WI, USA) and fast cycling
575 parameters, i.e., 10 minutes at 50 °C, 2 minutes at 95 °C, and 40 amplification cycles (95 °C for
576 3 seconds followed by 30 seconds at 60 °C). Viral RNA of the other flaviviruses was quantified
577 using 7.5 µL of RNA and 12.5 µL of RT-qPCR mix (SuperScript III Platinium one-step qRT-PCR
578 kit with Rox from Thermo Fisher Scientific, or GoTaq Probe one-step RT-qPCR system from
579 Promega) and standard cycling parameters, i.e., 20 minutes at 50 °C, 3 minutes at 95 °C and 40
580 amplification cycles (95 °C for 15 seconds followed by 1 minute at 60 °C)[18].

581 For the DENVs, RT-qPCR reactions were loaded on QuantStudio 12K Flex Real-Time PCR
582 System (Applied Biosystems, Waltham, MA) and analyzed using QuantStudio 12K Flex software
583 v1.2.3. For the other flaviviruses, RT-qPCR reactions were loaded on an ABI 7900 HT Fast Real-
584 Time PCR System (Applied Biosystems) and analyzed using SDS 1.2 Applied Biosystems
585 software. Viral RNA was quantified using serial dilutions of a standard curve consisting of four
586 2-log dilutions of an appropriate T7-generated RNA standard of known quantities for each
587 serotype or virus (100 copies to $100 \times 10^6$ copies). Inhibition values for each drug concentration
588 were plotted using KaleidaGraph plotting software (version 4.03; Synergy Software, Reading, PA)
589 and the best sigmoidal curve, fitting the mean values, was used for determination of the $EC_{50}$ value.
590 The $EC_{50}$ value was determined using logarithmic interpolation.

591 **DENV-2 *in vitro* resistance selection**

592 Vero cells were seeded at a density of $2 \times 10^5$ cells/well in a 24-well plate. Next day, cells were
593 infected (MOI = 0.01; virus stock was diluted 200×) with DENV-2 RL strain and incubated with
594 virus for 1.5 to 2 hours at 37 °C. Virus was then removed and cells were rinsed three times using
595 assay medium (MEM/2%FBS). Cells were further incubated in the presence of a 2-fold serial
596 dilution of JNJ-A07 (10 – 0.00002 µg/mL) for 7 days at 37 °C. After 7 days, cells were
597 microscopically checked for CPE and supernatant from two adjacent wells showing 30% to 70%
598 CPE was harvested and pooled. The $EC_{50}$ was microscopically determined as the average
599 concentration of the compound that was added to the two selected and pooled wells (showing 30-
600 70% CPE). The supernatant was used to infect freshly seeded cells using the same virus dilution
601 (i.e., 200×) as in all previous passages. The remaining supernatant was stored at -80 °C until further
602 analysis (i.e., sequencing and plaque assay). During weekly passaging of the virus, the start
603 concentration of the compound was gradually increased. In addition, a fresh compound solution
604 was used after each $10^{th}$ passage to prevent that the shift in $EC_{50}$ was the result of possible
605 instability of the compound. This procedure was repeated on a weekly basis until the observed
606 $EC_{50}$ value approached the cytostatic concentration of the compound. To check for spontaneous
607 and/or tissue culture-adapted mutations, part of the wells served as WT virus controls to which no
608 compound was added. WT DENV was passaged on Vero cells in a similar way as compound-
609 treated virus.

610 ***In vitro* growth kinetics of DENV resistant to JNJ-A07**

611 The growth kinetics of resistant viruses obtained via *in vitro* resistance selection with JNJ-A07 in
612 two independent efforts (A and B) was evaluated in both Vero E6 and C6/36 cells. Vero E6 cells
613 were seeded at a density of $4 \times 10^5$ cells/well in a 12-well plate. Next day, cells were infected with
614 either WT or compound-resistant DENV-2 RL (MOI of 0.1) diluted in MEM/2%FBS assay
615 medium. Cells were incubated for 2 hours at 37 ºC, after which the viral inoculum was removed,
616 and cells were washed twice with assay medium. Supernatant was collected on day 1 to 7 p.i.,
617 followed by the determination of the viral RNA load by RT-qPCR and plaque assay.

618 For evaluating the growth kinetics on C6/36 cells, the same procedure was followed with some
619 modifications. Cells were seeded at a density of $8 \times 10^5$ cells/well in a 12-well plate and infections
620 were performed using an MOI of 0.01. Supernatant was collected on day 1 to 10 p.i. for

621 quantification of the viral RNA load by RT-qPCR. On day 11 p.i., supernatant was collection for
622 determination of the infectious virus titers by plaque assay.

623 **Whole genome sequencing**

624 Viral RNA was isolated from cell culture supernatant (140 µL) using the QIAamp Viral RNA Mini
625 kit (Qiagen) per manufacturer's protocol with the exception that 5 µg of linear polyacrylamide
626 (Life Technologies) was used as the carrier instead of the carrier RNA provided with the kit. All
627 samples were subsequently treated with RNA clean & Concentrator-5 (DNAse incuded) (Zymo
628 Research). Viral RNA was amplified into double-stranded DNA using the Ovation RNA-Seq
629 version 2 kit (NuGEN, San Carlos, CA) per manufacturer's protocol. Paired-end libraries for
630 Illumina sequencing were prepared using the Nextera XT DNA Library Preparation Kit (Illumina)
631 per manufacturer's protocol. Prior to sequencing on a MiSeq (Illumina; 150 base paired reads),
632 short amplification products were removed using AMPure XP beads (Beckmann coulter).
633 Sequence reads were binned by index read prior to further analysis. Poor quality bases of each read
634 were trimmed prior to alignment. Sequences were filtered for viral content by aligning the reads
635 to genotype-specific viral genomes using the CLC genomics workbench (Qiagen). A custom
636 script[39] was used to derive the amino acid composition of each sample for all coding sequences
637 per DENV genotype. A coverage cut-off value of 100 and a 15% read frequency cut-off were used
638 for the reliable detection of amino acid variants.

639 **Transient mutant replication assays to study replication fitness and compound resistance**

640 A panel of mutant sub-genomic DENV reporter replicons (sgDVs-R2A) each harboring an NS4B
641 resistance mutation was used to determine the replication fitness and compound resistance
642 imposed by each of these mutations. First, each resistance mutation was inserted separately into
643 the sgDVs-R2A replicon. The plasmid (denoted pFK-sgDVs-R2A) contains the non-structural
644 genes NS1-NS5 of the DENV-2/16681 strain with cell-adaptive mutations in NS3 (A56V and
645 H451P), NS4A (I116M), and NS5 (E892K) in NS5, and the Renilla Luciferase (*rluc*) reporter
646 gene[34]. Mutations in the NS4B region were introduced by site-directed mutagenesis (SDM) using
647 the QuickChange II XL Site-Directed Mutagenesis Kit according to the instructions of the
648 manufacturer (Agilent), resulting in the respective mutant sgDVs-R2A expression plasmids.
649 Plasmid DNA was linearized with *Xba*I (located at the end of the 3' untranslated region of the viral
650 genome) and purified using the NucleoSpin Gel and PCR Clean-up kit (Macherey-Nagel). *In vitro*

651 transcription was performed with the mMESSAGE mMACHINE SP6 kit (Ambion) according to
652 the manufacturer's protocol. RNA was purified using acidic phenol chloroform extraction,
653 precipitated with isopropanol, and dissolved in RNase-free water. The molecular weight and
654 integrity were checked by agarose gel electrophoresis. Both wild-type and mutant sgDVs-R2A *in*
655 *vitro* transcribed RNA was transiently transfected into Huh-7 cells. To this end, 10 µg *in vitro*
656 transcribed linear RNA was electroporated into Huh-7 cells (electroporation at 975 µF and 270 V;
657 Gene Pulser II, Bio-Rad), as described previously[34,40]. To determine replication fitness, transfected
658 cells were transferred to prewarmed complete DMEM and seeded in duplicate into 6-well plates
659 at different densities depending on the incubation time ($2 \times 10^5$ cells for 4h- and 24h-incubations;
660 $1 \times 10^5$ cells for 48h- and 72h-incubations; $5 \times 10^4$ cells for a 96-h incubation). At the respective
661 time points, cells were washed once with PBS and lysed, as described previously[40]. Lysates were
662 frozen immediately at -20 °C. After collection of all samples, lysates were thawed, resuspended
663 by gentle pipetting, and luciferase activity was measured for 10 sec in a plate luminometer (Mithras
664 LB940, Berthold, Freiburg, Germany), as reported earlier[40]. To determine compound resistance,
665 transfected cells (4,000 cells/well in a 384-well plate) were incubated with serial dilutions of JNJ-
666 A07 at 37 °C. Two days post-transfection, viral replication was quantified by measuring luciferase
667 activity.

668 **Immunoprecipitation experiments**

669 Huh-7 cells stably expressing the T7 RNA polymerase and DENV2 NS2B-NS3 were seeded into
670 10 cm-diameter cell culture dishes ($2 \times 10^6$ cells/dish) 18 h prior to transfection. For each construct,
671 10 µg of plasmid DNA (plasmid encoding NS4A-2K-NS4B(-HA$^{Ct}$) with NS4B corresponding to
672 the WT or containing a JNJ-A07 resistance mutation (with or without a C-terminal HA tag) was
673 mixed with 800 µL Opti-MEM™, and 30 µL of TransIT®-LT1 Transfection reagent was added.
674 The mix was equilibrated at room temperature for 20 min and added in a drop-wise manner to the
675 cells. To study compound resistance, indicated concentrations of JNJ-A07 or an equivalent amount
676 of DMSO without compound was added to each plate along with the transfection mix. Medium
677 was replaced 4 h post-transfection by fresh DMEM supplemented with or without the same
678 concentration of JNJ-A07. Eighteen hours post-transfection, cells were first washed with PBS and
679 then collected. For studying the kinetics of JNJ-A07-induced block of the NS3-NS4B interaction,
680 transfection medium without compound was replaced after 4 h. JNJ-A07 (2.8 µL of a 100 µM

681 stock solution in DMSO) or an equivalent amount of DMSO was added either at 4 h or 24 h after
682 transfection. Cells were collected at 1 h, 8 h or 24 h post-treatment.

683 Harvested cells were lysed on ice for 20 min in 500 µL lysis buffer containing 150 nM NaCl, 50
684 mM NaF, 20 mM Tris (pH 7.5), 0.5% dodecyl beta-D maltoside (DDM; w/v) and protease
685 inhibitors (Roche). To remove cell debris, lysates were centrifuged in a pre-cooled (4 °C) benchtop
686 centrifuge for 45 min at maximum speed (21,130 × *g*). A Bradford Assay was used to determine
687 the protein concentration of each sample and samples were adjusted to the one with the lowest
688 concentration. For HA-specific immunoprecipitation, 30 µL of equilibrated mouse monoclonal
689 anti-HA agarose beads (antibody concentration is 2.1 mg/ml settled resin, as specified by the
690 manufacturer; A2095, Sigma-Aldrich) was added to each sample and incubated for 3 h at 4 °C.
691 Beads were washed twice with lysis buffer and twice with PBS, and captured proteins were eluted
692 in a first step with PBS containing 5% sodium dodecyl sulfate (SDS), followed by an elution step
693 with pure PBS. Four sample volumes of acetone were added to combined eluates to perform
694 overnight precipitation of proteins at -20 °C. Samples were centrifuged at 4 °C for 1 h at 21,130 ×
695 *g*. Pellets were air-dried, resuspended in SDS sample buffer and loaded onto an SDS-
696 polyacrylamide gel. After electrophoresis, proteins were transferred onto an Amersham Protran
697 0.2 µm nitrocellulose membrane (GE Healthcare Life Sciences, Little Chalfont, UK) for Western
698 blotting and analyzed by using a chemoluminescence imager (ECL ChemoCam Imager, Intas
699 Science Imaging Instruments GmbH, Göttingen, Germany), as described previously[19,20]. NS4B-
700 and NS3-specific bands were visualized by using in-house generated rabbit polyclonal antibodies
701 directed against respectively NS4B (1:1,000 dilution) or NS3 (1:2,000 dilution), as described
702 previously[19,20,30]. Glyceraldehyde-3-phosphate dehydrogenase (GAPDH) or β-actin served as
703 loading controls for cell lysates (input), which were visualized by using the mouse monoclonal
704 anti-GAPDH antibody (1:1,000 dilution; sc-365062, Santa Cruz Biotechnology) or the mouse
705 monoclonal anti-β-actin (1:5,000 dilution; A5441, Sigma-Aldrich), respectively. Intensities were
706 quantified using ImageJ2 (version 1.53j, Fiji). Statistical analysis was conducted using either "R"
707 script or GraphPad Prism 7.04 software package (LaJolla, USA) and is specified in further detail
708 in the legends of the respective figures. The treatment effect of JNJ-A07 on protein ratios was
709 assessed by means of linear mixed effects models. In addition, a random effect for replicates was
710 included. 95% confidence intervals were provided, indicating the variability on the estimated
711 effects. Sidak's multiplicity correction was applied to the intervals to account for multiple testing.

712 **Immunoprecipitation of NS4B-HA containing complexes ('*in cellulo* assay')**

713 Huh-7 cells were infected with DENV-2(NS4B-HA*), which is a replication-competent DENV
714 carrying an internal HA tag in the NS4B protein[20], or DENV-2 WT as a control (MOI = 1). Forty-
715 eight hours p.i., cells were treated for various time spans (1 h, 6 h, 24 h) with either 500 nM of
716 Analogue 2 or buffer with an equivalent concentration of DMSO. Cells were collected, lysed in
717 DDM lysis buffer and subjected to immunoprecipitation using the HA affinity tag. Captured
718 complexes were analyzed by Western blot and intensities of NS4B- and NS3-specific bands were
719 quantified using the ImageJ2 software package (Fiji).

720 ***In vitro* drug assay**

721 Huh-7 cells stably expressing the T7 RNA polymerase and DENV-2 NS2B-NS3 were transfected
722 with pTM1-NS4A-2K-NS4B(-HA$^{Ct}$) constructs using TransIT-LT1 (Mirus, Madison, WI, USA),
723 according to the manufacturer's protocol (800 µL serum-free OPTi-MEM medium, 10 µg DNA,
724 30 µL TransIT-LT1). After 4 h, medium was exchanged for fresh DMEM and 30 h post-
725 transfection, cells were collected, washed and resuspended in DDM lysis buffer. Lysates were
726 treated with either 1 µM Analogue 2 or an equal volume of DMSO and then incubated at various
727 temperatures for 2 h. HA-specific complexes were analyzed as described above.

728 **Pharmacokinetic studies**

729 All animal studies were performed with the approval of and under the guidelines of the Ethical
730 Committee. The pharmacokinetic profile was evaluated in fed male CD-1 mice ($n$ = 3 per group,
731 6-8 weeks old; Charles River Laboratories). Mice were intravenously injected with 2.5 mg/kg of
732 the test compound, which was formulated as an 0.5 mg/mL solution in polyethylene glycol 400
733 (PEG400):water + NaOH (50:50), and blood samples were collected (in EDTA-containing micro-
734 centrifuge tubes) from the dorsal metatarsal vein at 0.12, 0.33, 1, 2, 4 and 7 h after dosing, or via
735 heart puncture at 24 h after dosing. Additionally, test compound was administered by oral gavage
736 at 1, 3, 10 and 30 mg/kg, formulated as a solution in PEG400:water + NaOH (50:50), and blood
737 samples were collected from the dorsal metatarsal vein at 0.5, 1, 2, 4 and 7 h after dosing, or via
738 heart puncture at 24 h after dosing. Blood samples were immediately centrifuged at 4 °C and
739 plasma was stored at -20 °C. Compound concentrations in the plasma samples were determined
740 using an API 4000 LC-MS/MS System mass spectrometer (Applied Biosystems). Individual

741 plasma concentration-time profiles were subjected to a non-compartmental pharmacokinetic
742 analysis (NCA) using Phoenix™ WinNonlin version 6.1. (Certara, NJ, USA).

743 **DENV-2 infection models in mice**

744 Breeding couples of AG129 mice (129/Sv mice deficient in both IFN-α/β and IFN-γ receptors)
745 were purchased from Marshall BioResources and bred in-house. The SPF status of the mice was
746 regularly checked at the KU Leuven animal facility. Mice (maximum 5 mice per cage, type GM500)
747 were housed in individually ventilated cages (Sealsafe Plus, Tecniplast) at 21 °C, 55% humidity
748 and 12:12 light/dark cycles. Mice were provided with food and water ad libitum as well as with
749 cardboard play tunnels and cotton as extra bedding material. Allocation to experimental groups
750 was performed randomly.

751 Housing conditions and experimental procedures were approved by the ethical committee of KU
752 Leuven (license P169/2011 and P047/2017), following institutional guidelines approved by the
753 Federation of European Laboratory Animal Science Associations (FELASA). AG129 mice were
754 used to assess the activity of JNJ-A07 on viral RNA levels in plasma and several tissues (spleen,
755 kidney, and liver). To this end, female mice (7-11 weeks old, $n$ = 8 per group) were challenged
756 intraperitoneally (i.p.) with $10^6$ PFU DENV-2 RL strain. Mice were treated twice daily (b.i.d.) by
757 oral gavage for 3 consecutive days with either vehicle (PEG400:water + NaOH (50:50)) or various
758 doses of JNJ-A07 (i.e., 30, 10, 3 or 1 mg/kg/dose), with the first administration one hour before
759 DENV challenge. On day 3 p.i., mice were euthanized, and blood, spleen, kidney and liver were
760 collected and stored at -80 °C until further use. Viral RNA isolation from plasma and tissues was
761 performed as described before[41].

762 To monitor the effect of the compound on viral RNA levels in the blood on various days p.i., an
763 *in vivo* kinetics study was performed. AG129 mice (7-11 weeks old, females, $n$ = 16 per group)
764 were inoculated i.p. with $10^2$ PFU DENV-2 RL strain. Mice were treated twice daily via oral
765 gavage with vehicle or JNJ-A07 using five different doses: 30, 10, 3, 1 and 0.3 mg/kg. Treatment
766 was initiated 1 hour prior to DENV infection and continued for 6 consecutive days. Each group
767 was sub-divided in two smaller groups ('A' and 'B'; $n$ = 8 each), from which blood was collected
768 on alternating days: on day 1, 3 and 5 for the A groups, and on day 2, 4 and 6 for the B groups. On
769 day 8 and day 11 p.i., mice from the A and B groups, respectively, were euthanized and blood,
770 spleen, kidney, and liver were collected and stored at -80 °C until further use.

771 The protective effect of JNJ-A07 on the development of virus-induced disease was assessed in a
772 lethal DENV challenge model (or 'survival' study). To mimic ADE-induced dengue disease,
773 AG129 mice (7-11 weeks old, females, *n* = 10 per group) were injected i.p. with 100 µL (1:50
774 diluted) Anti-Flavivirus Group Antigen Antibody, clone D1-4G2-4-15 ('4G2'; Millipore) one day
775 prior to challenge with DENV-2 RL strain ($10^6$ PFU, i.p.). Mice were treated twice daily by oral
776 gavage with either vehicle or JNJ-A07 at a dose of 30, 10, 3, or 1 mg/kg. Treatment was initiated
777 1 hour prior to DENV challenge and continued for 5 consecutive days. On day 3 p.i., blood was
778 collected for the quantification of viral RNA levels (only during one of the two studies). Mice were
779 observed daily for body weight loss and the development of virus-induced disease. When reaching
780 humane endpoints (body weight loss of ≥20%, hunched posture, ruffled fur, conjunctivitis,
781 movement impairment, lower limb paralysis), mice were euthanized with pentobarbital. On day
782 25 p.i., the study was ended, and all surviving mice were euthanized with pentobarbital.

783 In delayed-treatment studies, AG129 mice (7-11 weeks old, females, *n* = 8 per group) were
784 inoculated i.p. with $10^2$ PFU DENV-2 RL strain. Treatment with JNJ-A07 (30 mg/kg, b.i.d.) was
785 initiated on various days: day 1, 2, 3, 4, 5, or 6 p.i., and continued for 6 days. Mice treated with
786 vehicle or JNJ-A07 whereby treatment was initiated on the day of infection (i.e., 1 hour prior to
787 infection) were included as controls. Each group was sub-divided in two smaller groups ('A' and
788 'B'; *n* = 4 each), from which blood was collected on alternating days: on day 1, 3, 5, and 7 p.i. for
789 the A groups, and on day 2, 4, 6, and 8 p.i. for the B groups. On day 12 and day 14 p.i., mice from
790 the A and B groups, respectively, were euthanized and blood was collected and stored at -80 °C
791 until further use.

792 **Cytokine measurement**

793 Induction of pro-inflammatory cytokines was analyzed in 20 µl plasma using the mouse cytokine
794 11-plex antibody bead kit (ProcartaPlex Mouse Th1/Th2 Cytokine Panel 11plex; EPX110-20820-
795 901), which measures the expression of TNF-α, IFN-γ, GM-CSF, IL-1β, IL12p70, IL-2, IL-4, IL-
796 5, IL-6, IL-13, and IL-18. Measurements were performed using a Luminex 100 instrument
797 (Luminex Corp., Austin, TX, USA) and were analyzed using a standard curve for each molecule
798 (ProcartaPlex). Statistical analysis was performed using a two-sided Kruskal-Wallis test, preceded
799 by the identification of outliers using the two-sided Grubbs' test ($\alpha$ = 0.05) in GraphPad Prism

800 (GraphPad Software 9.0.0). *P* values were adjusted using the Dunn's multiple comparisons
801 correction method.

802 **Statistical analysis *in vivo* studies**

803 Statistical power calculations considered the number of mice required to detect a significant
804 reduction in viremia compared to vehicle-treated controls. With groups of $n = 8$, a reduction of at
805 least $0.8\log_{10}$ in viral RNA can be detected, according to the independent t-test (with $\alpha = 0.05$,
806 power = 80% and an SD value of 0.5). In addition, statistical calculations considered the number
807 of mice required to detect a significant improvement in survival compared to vehicle-treated
808 controls. With groups of $n = 11$, a minimal survival rate of 60% for treated animals versus 0% in
809 the untreated, infected control group can be demonstrated, according to the Fisher's exact test (with
810 $\alpha = 0.05$ and power = 80%). The experiments were not randomized, and investigators were not
811 blinded to allocation during experiments and outcome assessment.

812 To assess the effect of JNJ-A07 treatment on viral load in plasma, spleen, kidney and liver for each
813 treatment group compared to the vehicle-treated animals (viremia studies), the two-sided Kruskal-
814 Wallis test was applied. *P* values from the Kruskal-Wallis test were adjusted using the Holm's
815 multiple comparisons correction method. To assess the effect of JNJ-A07 treatment on viral load
816 in plasma for each treatment group compared to the vehicle-treated mice that were treated with the
817 Anti-Flavivirus Group Antigen Antibody ('Viremia + 4G2 Ab'), a Tobit regression model was
818 applied. The (two-sided) *P* values were adjusted using the Bonferroni's multiple comparisons
819 correction method. For the viral kinetics studies and the delayed-treatment studies, a batch
820 approach was applied to calculate the viral load area under the curve (AUC) using the PK R
821 package[42]. This package estimates an average AUC value for settings where subjects are measured
822 at varying time points within a treatment group. Within each experiment, the mean AUC value and
823 95% CI was determined for each group. The AUC was calculated using the limit of detection
824 (LOD; 2.6 $\log_{10}$ copies/mL) as the lowest limit. In case the CI of a compound-treated group
825 overlapped with that of the vehicle-treated group, the groups were considered not to differ
826 significantly. In case the CIs did not overlap, the groups were considered to differ significantly. In
827 the delayed treatment studies, the viral load AUC for each of the compound-treated groups was
828 calculated from the day treatment was initiated until the end of the study and compared to that of
829 the vehicle-treated group. The Fisher's exact test was used to determine if the survival rate on day

830 25 for each compound treatment group differed significantly from that of the vehicle group. *P*
831 values were adjusted using the Holm's multiple comparisons correction method. *P* values of ≤0.05
832 were considered significant and *P* values lower than 0.0001 are depicted as *P*<0.0001 in the graphs.

833 **References in Methods**


834 34. Fischl, W. & Bartenschlager, R. High-throughput screening using dengue virus reporter
835 genomes. *Methods Mol. Biol.* **1030**, 205-219 (2013).

836 35. Aubry, F. *et al*. Single-stranded positive-sense RNA viruses generated in days using infectious
837 subgenomic amplicons. *J. Gen. Virol.* **95**, 2462-2467 (2014).

838 36. Kum, D. B. *et al.* A yellow fever-Zika chimeric virus vaccine candidate protects against Zika
839 infection and congenital malformations in mice. *NPJ Vaccines* **3**, 56 (2018).

840 37. De Burghgraeve, T. *et al.* 3',5'Di-O-trityluridine inhibits in vitro flavivirus replication.
841 *Antiviral Res.* **98**, 242-247 (2013).

842 38. Kaptein, S. J. F. *et al.* A derivate of the antibiotic doxorubicin is a selective inhibitor of dengue
843 and yellow fever virus replication in vitro. *Antimicrob. Agents Chemother.* **54**, 5269-5280
844 (2010).

845 39. Verbist, B. M. *et al.* VirVarSeq: a low-frequency virus variant detection pipeline for Illumina
846 sequencing using adaptive base-calling accuracy filtering. *Bioinformatics* **31**, 94-101 (2015).

847 40. Münster, M *et al*. A Reverse Genetics System for Zika Virus Based on a Simple Molecular
848 Cloning Strategy. *Viruses* **10**, E368 (2018).

849 41. Zmurko, J. *et al.* The Viral Polymerase Inhibitor 7-Deaza-2'-*C*-Methyladenosine Is a Potent
850 Inhibitor of In Vitro Zika Virus Replication and Delays Disease Progression in a Robust
851 Mouse Infection Model. *PLoS Negl. Trop. Dis.* **10**, e0004695 (2016).

852 42. Jaki, T. & Wolfsegger, M. J. Estimation of pharmacokinetic parameters with the R package
853 PK. *Pharm. Stat.* **10**, 284-288 (2011).


854 **Data Availability**

855 The genome sequence of DENV-2 Rega Labstrain (or DENV-2 RL) is deposited at GenBank
856 (Accession number MW741553). The synthesis and chemical characterization of all compounds
857 described in this paper is provided as Supplementary Information (Supplementary Methods). The

858 uncropped images of the Western blots shown in Figure 1, Extended Data Figure 5 and Extended
859 Data Figure 6 are presented in Supplementary Figures 1-6. All data supporting the findings of this
860 study are available within the article, the Source data or the Supplementary Information provided
861 with this article.

862 **Code availability**

863 A custom script[39] was used to derive the amino acid composition of each sample for all coding
864 sequences per DENV genotype, which was not specifically developed for this research but for all
865 similar analyses. The code for the custom script is deposited as part of the pipeline VirVarSeq but
866 is individually accessible on the Open Source software platform SourceForge at
867 https://sourceforge.net/projects/virtools/?source=directory. The code for this specific variant
868 detection script is 'codon_table.pl'. Graphs and figures were generated using Microsoft
869 PowerPoint, GraphPad Prism (version 9.0.0; LaJolla, USA), or Adobe Illustrator (version 25.4.1;
870 San Jose, USA); the software is made available by KU Leuven through a group license. In some
871 figures, basic templates obtained from the Sevier Medical Art library (https://smart.servier.com/)
872 were used.

873 **Acknowledgements**

874 This work was supported by a Seeding Drug Discovery Strategic Award from the Wellcome Trust
875 (grant 089328/Z/09 and grant 106327/Z/14) and received funding from the Flanders Agency
876 Innovation & Entrepreneurship (VLAIO O&O grants IWT 150863 and HBC.2019.2906). Part of
877 this research work was performed using the 'Caps-It' research infrastructure (project ZW13-02)
878 that was financially supported by the Hercules Foundation (FWO) and Rega Foundation, KU
879 Leuven. We would like to thank Mieke Flament, Ruben Pholien, Carolien De Keyzer, Charlotte
880 Vanderheydt, Elke Maas, Sandra Claes, and the Rega animal facility at KU Leuven; Elien Peeters,
881 Suzanne De Bruyn, Nick Verheyen, Carl Van Hove, Erwin Coesemans, Benoit De Boeck, Andrea
882 Beckers, Petra Gysemberg, Tine Loomans and Kathleen Allaerts at Janssen Pharmaceutica; and
883 Jérôme Fortin, Frédéric Doublet and Philippe Muller at Janssen-Cilag for technical assistance.

884 **Author Contributions**

885 S.J.F.K. and J.N.: Planning, coordination and execution of experimental virology work at KU
886 Leuven; O.G. and M.V.L.: Planning, coordination and execution of experimental virology work at

887 Janssen Pharmaceutica; P.G.: Execution of experimental virology work at Janssen Pharmaceutica.
888 D.K., L.C-C., M.M. and R.B.: Planning, coordination and execution of experimental virology work
889 at Heidelberg University; D.B.: Planning, coordination and execution of medicinal chemistry work
890 at Cistim; K.D.: Experimental work at KU Leuven and advise on design of experiments; K.T.:
891 Whole genome sequence analysis at Janssen Pharmaceutica; M.C.: Statistical analysis at Janssen
892 Pharmaceutica.; G.Q., F.T. and X.D.L: Planning, coordination and execution of experimental work
893 at UVE; B.K., J-F.B., T.H.M.J. and P.R.: Planning, coordination and execution of medicinal
894 chemistry work at Janssen Pharmaceutica; B.S.: Planning and coordination of PK-PD work at
895 Janssen Pharmaceutica; A.M. and P.C.: Coordination and guidance of experimental medicinal
896 chemistry work at CD3; P.C. and J.N.: Designed and initiated project; K.S. and M.V.L.: Initiated
897 project at Janssen Pharmaceutica; J.N., P.C., A.M., S.J.F.K., O.G., R.B., M.V.L. and K.S.: securing
898 of funding from external organizations. S.J.F.K., O.G., M.V.L. and J.N. wrote the manuscript with
899 contributions from K.S., D.K. and R.B., and comments from all authors.

900 **Competing interests**

901 S.J.F.K., O.G., A.M., B.K., J-F.B., D.B., B.S., T.H.M.J., K.D., P.R., K.S., P.C., M.V.L. and J.N.
902 have filed a patent application claiming the discovery of this class of antiviral molecules as dengue
903 viral replication inhibitors (WO2017/167951). The remaining authors declare no competing
904 interests.

905 **Additional information**

906 **Supplementary Information** is linked to the online version of the paper at
907 www.nature.com/nature.

908 **Correspondence and requests for materials** should be addressed to J.N. and M.V.L.

909 **Reprints and permissions information** is available at www.nature.com/reprints.

910

911 **Extended Data Fig. 1 Dose-response curves of the antiviral activity of JNJ-A07 against**
912 **DENV-2 on various cell types. a-f**, The antiviral effect (% Inhibition viral RNA replication, %
913 Inhibition eGFP expression, or % Inhibition of infected cells) is depicted by white dots. The effect
914 of JNJ-A07 on cell growth is depicted by grey dots. Assays were performed on Vero cells (**a** and
915 **c**), Huh-7 hepatoma cells (**b**), C6/36 mosquito cells (**d**), human monocytic leukemia THP-1 cells
916 expressing the DC-SIGN receptor (**e**), and immature dendritic cells (imDCs) (**f**). Cells were
917 infected with either the DENV-2/16681/eGFP strain (**a**-**b**, **e**), DENV-2/16681 (**f**) or the DENV-2
918 RL strain (**c**-**d**). Data represent average values ± s.d. from two (for Vero and C6/36 cells using
919 DENV-2 RL, and for imDCs using DENV-2/16681), three (for THP-1/DC-SIGN cells using
920 DENV-2/16681), and at least five (for Vero and Huh-7 cells using DENV-2/16681) independent
921 experiments.

922 **Extended Data Fig. 2 JNJ-A07 is highly specific for DENV. a**, Antiviral activity of JNJ-A07
923 against various of RNA and DNA viruses. CHIKV, chikungunya virus; HadV, human adenovirus;
924 HBV, hepatitis B virus; HCV, hepatitis C virus; HIV, human immunodeficiency virus; hRV,
925 human rhinovirus; IVA, influenza virus A; IVB, influenza virus B; RSV, respiratory syncytial
926 virus; rVSV, recombinant vescular stomatitis virus; VACV, vaccinia virus; JEV, Japanese
927 encephalitis virus; WNV, West Nile virus; YFV, yellow fever virus; ZIKV, Zika virus. ND, not
928 determined. **b**, NS4B sequence alignment of related flaviviruses. The NS4B protein sequence of
929 DENV-2/16681 was aligned with corresponding sequences from JEV strain JEV CNS769 Laos
930 2009 (GenBank KC196115), tick-borne encephalitis virus strain Oshima 5.10 polyprotein gene
931 (GenBank MF374487), WNV isolate R94224 CDC polyprotein gene (GenBank MF004388), YFV
932 isolate Bolivia 88 1999 polyprotein gene (GenBank MF004382) and ZIKV strain HPF 2013
933 (GenBank KJ776791) using Clustal Omega Version 2.1. Post-processing was conducted with
934 Jalview 2.11.1.3. The DENV NS4B topology model was added manually based on Miller *et al*.[30].
935 Black arrowheads are pointing at locations associated with compound-resistance.

936 **Extended Data Fig. 3 Time-of-drug-addition and *in vitro* resistance selection. a**, Experimental
937 setup of the time-of-drug-addition assay (TOA). **b**, TOA and *in vitro* kinetics of DENV-2
938 replication. *In vitro* DENV RNA replication in the absence of compound is depicted by the red
939 curve. Onset of intracellular viral replication is at 10 hours p.i., as shown in the inset. The inhibitory
940 effect of JNJ-A07 on DENV replication when added at different time points p.i. is depicted by the
941 blue curves (0.0001 μM, light blue; 0.001 μM, dark blue). The broad-spectrum RNA virus

942 inhibitor 7-deaza-2'-*C*-methyladenosine (7DMA) served as positive control (black curve with
943 white circles). Data (average ± s.d.) from at least three independent experiments. **c**, Experimental
944 approach of *in vitro* resistance selection. **d-e**, The dynamics of appearance of mutations was
945 studied using whole genome sequencing. JNJ-A07 selected for mutations in NS4B, which were
946 not present in the wild-type (WT) viruses that were passaged along without any drug pressure, of
947 two independently selected resistant strains. Results for the A and B sample are shown in (**d-e**),
948 respectively. Each colored line shows the dynamics of appearance of a certain mutation during
949 passaging of the virus in presence of JNJ-A07; the mutation is depicted in the same color. Whole
950 genome sequencing was performed on DENV variants harvested at every $5^{th}$ passage (P) and at
951 the end of the experiment (i.e., passage 43). One passage represents a one-week time span. The
952 dotted line represents the cut off (15%) for the detection of variants compared with WT in the virus
953 population. The increasing $EC_{50}$ values, as determined by microscopic evaluation of virus-induced
954 CPE, are depicted below the graphs. **f**, Mutations in DENV NS4B identified at endpoint after *in*
955 *vitro* resistance selection using JNJ-A07 and Analogue 1. **g**, Natural occurrence of the NS4B
956 mutations in clinical isolates.

957 **Extended Data Fig. 4 Replication properties of resistant subgenomic replicons and DENV**
958 **strains. a**, Schematic representation of the subgenomic DENV-2/16681 reporter replicon sgDVs-
959 R2A[34]. **b**, Effect of resistance mutations in NS4B on replication fitness. Resistance mutations
960 identified in Extended Data Fig. 3 were introduced into sgDVs-R2A. A replication-deficient
961 replicon containing an inactivating mutation in the NS5 RNA-dependent RNA polymerase domain
962 (GND) served as negative control. Huh-7 cells were transfected with *in vitro* transcribed RNA of
963 WT or mutant sgDVs-R2A and lysed at the time points given at the top right and Renilla luciferase
964 activity was measured as marker of replication. Relative light units (RLU) were normalized to the
965 4 h value, reflecting transfection efficiency. Plotted are the average ± s.d. from at least three
966 independent experiments, each carried out with independent RNA preparations. **c**, *In vitro* growth
967 kinetics of resistant DENV (blue bars) compared to WT DENV (grey bars) on Vero E6 cells for
968 the A sample. The virus titer in the supernatant was determined by plaque assay. **d**, *In vitro* growth
969 kinetics of resistant DENV (blue bars) compared to WT DENV (grey bars) on C6/36 cells for the
970 A sample. Viral RNA load in the supernatant was determined by RT-qPCR. **e**, Infectious virus on
971 day 11 p.i. in the supernatant of C6/36 cells infected with resistant DENV (blue bars) or WT DENV
972 (grey bars) for the A sample, as determined by plaque assay. **f**, *In vitro* growth kinetics of resistant

973 DENV (dark blue bars) compared to WT DENV (light grey bars) on C6/36 cells for the B sample.
974 Viral RNA load in the supernatant collected on day 1-10 p.i. was determined by RT-qPCR. Data
975 are from a single experiment (**d-f**) or average values ± s.d. from three independent experiments (**c**).
976 LOD, limit of detection; LLOQ, lowest limit of quantification.

977 **Extended Data Fig. 5 Impact of JNJ-A07 on the interaction between NS3 and various NS4B**
978 **species. a**, Experimental design to study the impact of JNJ-A07 on the interaction between NS3
979 and WT or mutant NS4B. **b**, Captured protein complexes were analyzed by Western blot. A
980 representative Western blot is shown. **c-d**, Western blot analysis to determine the NS3-NS4B
981 interaction strength. The uncropped images of **b-d** are presented in Supplementary Fig. 1-3.
982 Numbers on the left are molecular weights (kDa). GAPDH served as loading control for cell lysates
983 (input). **e-g**, Signal intensities (from three independent blots) of NS3, 4A-2K-NS4B, 2K-NS4B
984 and NS4B were normalized to WT NS4A-2K-NS4B-HA$^{Ct}$ in DMSO-treated control cells. Protein
985 ratios (average ± s.e.m.) were calculated for each sample. Repeated measures one-way ANOVA
986 with subsequent Dunnett's multiple comparisons test was used for statistical analysis. *ns*, not
987 significant. **h-j**, Protein intensities (average ± s.e.m.; three independent experiments) for WT (**h**)
988 and compound-resistant NS4B-mutants V91A (**i**) and T108I (**j**), normalized to an untreated WT
989 control. For statistical analysis, JNJ-A07-treated samples were compared with the corresponding
990 untreated control (left of the dashed line) using ordinary one-way ANOVA with subsequent
991 Dunnett's multiple comparisons test. **k**, $EC_{50}$ values (average ± s.e.m.) for protein ratios in (**e-g**)
992 obtained by fitting four-parameter dose-response curves to the results from each individual
993 experiment. Fold change in $EC_{50}$ is the ratio between the average $EC_{50}$ for WT and the respective
994 mutant constructs. **l**, JNJ-A07 potentially slows down the processing dynamics of the NS4A-2K-
995 NS4B precursor (illustrated by the hourglass icon), which is first cleaved by the NS2B-NS3
996 protease at the NS4A-2K cleavage site. 2K-NS4B is subsequently processed by the host signal
997 peptidase complex into mature NS4B and 2K.

998 **Extended Data Fig. 6 JNJ-A07 does not disrupt existing NS3-NS4B complexes. a**,
999 Experimental setup to study the kinetics of JNJ-A07-induced block of the NS3-NS4B interaction.
1000 **b**, Impact of JNJ-A07 on forming or pre-formed NS3-NS4B complexes. Huh-7 T7 NS2B-NS3
1001 cells treated with 0.035 μM JNJ-A07 or equal amounts of DMSO were harvested at 1, 8, or 24 h
1002 after drug addition. Lysates were subjected to HA-specific pull-down and analyzed by Western

1003 blot (enrichment factor 5). A representative Western blot is shown. Numbers on the left represent
1004 molecular weights (kDa). **c,** Experimental setup of the *in cellulo* assay, in which Huh-7 cells were
1005 infected with DENV-2(NS4B-HA*)[20] at an MOI of 1. At 48 h p.i., cells were treated for given
1006 periods with 500 nM of Analogue 2 or DMSO. **d**, NS3-NS4B complexes were enriched by NS4B-
1007 HA* pull-down and total lysates (input) and immune complexes (pull-down) were analysed by
1008 Western blot. NS3/NS4B ratios (depicted below the picture) were normalized to non-drug treated
1009 samples ($n$ = 1). **e**, Experimental setup of the *in vitro* drug assay to investigate the effect of the
1010 drug on established NS3-NS4B complexes. Cell lysates were treated with 1 µM of Analogue 2 or
1011 equal amounts of DMSO added to the lysis buffer and incubated for 2 h at different temperatures
1012 in order to test complex stability. Subsequently, NS4B-HA$^{Ct}$ pull-down was performed. **f,** Western
1013 blot analysis ($n$ = 1) analogous to the one shown in (**d**). The lower protein amount observed with
1014 the sample incubated at 37 °C was most likely due to proteolytic degradation in spite of adding
1015 protease inhibitors. For uncropped images of the representative blots in (**b**, **d**, **f**), see
1016 Supplementary Fig. 4-6. GAPDH (**b**, **f**) or β-actin (**d**) served as loading control for cell lysates
1017 (input).

1018 **Extended Data Fig. 7 *In vivo* efficacy of JNJ-A07 on viral RNA and cytokine levels. a-c**,
1019 Inhibitory effect of JNJ-A07 on viral RNA levels in spleen (**a**), kidney (**b**) and liver (**c**) on day 3
1020 p.i. from AG129 mice treated twice-daily with 30 (white dots), 10 (light blue dots), 3 (dark blue
1021 dots) or 1 (grey dots) mg/kg JNJ-A07, as compared to vehicle-treated mice (red dots). Data are
1022 from two independent studies with $n$ = 8 per group in each study. **d-g**, IL-18 (**d**), IFN-γ (**e**), TNF-
1023 α (**f**), and IL-6 (**g**) levels in plasma on day 3 p.i. (from one of the viremia studies in Fig. 2b). **h**,
1024 Inhibitory effect of JNJ-A07 on viral RNA levels in plasma on day 3 p.i. in the survival study (also
1025 see Fig. 2c). Dosing groups were similar to those in (**a-c**). Treatment started 1 hour before infection.
1026 Mice were injected with the Anti-Flavivirus antibody one day before infection. Data are from one
1027 study with $n$ = 10 per group. **i**, Inhibitory effect of NITD-688 on viral RNA levels on day 3 p.i. in
1028 AG129 mice treated twice-daily with 100 (yellow dots), 30 (white dots), 10 (light blue dots) or 3
1029 (dark blue dots) mg/kg NITD-688, as compared to vehicle-treated mice (red dots). Treatment
1030 started 1 hour before infection. Data are from one study with $n$ = 8 per group. Individual data and
1031 median values are presented. Undetermined Ct values were imputed at a Ct value of 40 (=LOD),
1032 corresponding to 2.6$\log_{10}$ viral RNA copies/mL. Statistical analysis was performed using the two-
1033 sided Kruskal-Wallis test (**a-c**, **i**) or a Tobit regression model (**h**). $P$ values were adjusted using the

1034 Holm's (**a-c**), Dunn's (**d-g**) or Bonferroni's (**h-i**) multiple comparisons correction method. *ns*, not
1035 significant, as compared to vehicle-treated mice. LLOQ, lowest level of quantification.

1036 **Extended Data Fig. 8 Efficacy of JNJ-A07 in the *in vivo* kinetics study. a**, Schematic outline
1037 of the *in vivo* kinetics study. Each treatment group was sub-divided in group A and B ($n$ = 8, each)
1038 for blood collection on alternating days. **b**, Weight curves (average values ± s.d.) of AG129 mice
1039 for the different treatment groups during the *in vivo* kinetics study (two independent studies).
1040 Colors of the dots represent the different treatment groups, as specified in (**c-g**). **c-g**, Inhibitory
1041 effect of JNJ-A07 on viremia on various days p.i. in mice treated twice-daily with 30 mg/kg (white
1042 dots, $n$ = 8), 10 mg/kg (light blue dots, $n$ = 8), 3 mg/kg (dark blue dots, $n$ = 16), 1 mg/kg (grey
1043 dots, $n$ = 8), or 0.3 mg/kg (green dots, $n$ = 8) JNJ-A07, as compared to vehicle-treated mice (red
1044 dots, $n$ = 16). Treatment was initiated 1 hour before intraperitoneal infection. Data (median ± s.d.)
1045 are from two independent studies. Undetermined Ct values were imputed at a Ct value of 40 (=limit
1046 of detection), corresponding to 2.6$\log_{10}$ viral RNA copies/mL. The mean AUC value and 95% CI
1047 was determined for each group. In case the CIs did not overlap, groups were considered to differ
1048 significantly. LLOQ, lowest level of quantification.

1049 **Extended Data Table 1 Antiviral activity of analogues of JNJ-A07 and NITD-688 against**
1050 **DENV-2.**

1051 *Selectivity index (SI) was calculated by dividing the average $CC_{50}$ value by the average $EC_{50}$
1052 value.

1053 Data represent average values ± s.d. from at least four independent experiments using DENV-
1054 2/16681 on Vero cells. Data for JNJ-A07, which are also shown in Table 1, were added to the table
1055 for comparative reasons. $EC_{50}$, 50% effective concentration; $CC_{50}$, 50% cytotoxic concentration.

1056 **Extended Data Table 2 Pharmacokinetic properties of JNJ-A07 in mice and rats after**
1057 **intravenous (a) and oral (b) dosing.**

1058 JNJ-A07 was administered to male CD-1 mice (6-8 weeks old) intravenously as a solution
1059 formulated in PEG400/water + NaOH (1:1) at 2.5 mg/kg or via oral gavage as a solution
1060 formulated in PEG400/water + NaOH (1:1) at 1, 3, 10 or 30 mg/kg. JNJ-A07 was administered to
1061 male Sprague Dawley rats (7-9 weeks old) intravenously as a solution formulated in PEG400/water
1062 (70/30) at 2.5 mg/kg or orally as a solution formulated in PEG400 at 10 mg/kg. Values represent

1063 average ± s.d. from 3 animals. F was calculated using $AUC_{(0\text{-inf})}$. A tolerability study was
1064 conducted with JNJ-A07 in male rats ($n$ = 5) at single doses of 0, 100, 300 and 1,000 mg/kg as a
1065 solution in PEG400. $CL_p$, plasma clearance; $V_{dssp}$, Volume of distribution in plasma at steady state;
1066 $t_{1/2}$, terminal phase elimination half-life; AUC, area under the plasma concentration versus time
1067 curve; $AUC_{(0\text{-last})}$, AUC up to the last measurable concentration; $AUC_{(0\text{-inf})}$, AUC curve to infinite
1068 time; $C_{max}$, maximum plasma concentration; $T_{max}$, the time to reach $C_{max}$; F, bioavailability; MTD,
1069 maximum tolerated dose; PEG400, polyethylene glycol 400; ND, not determined.
1070

1071 **Figure 1**

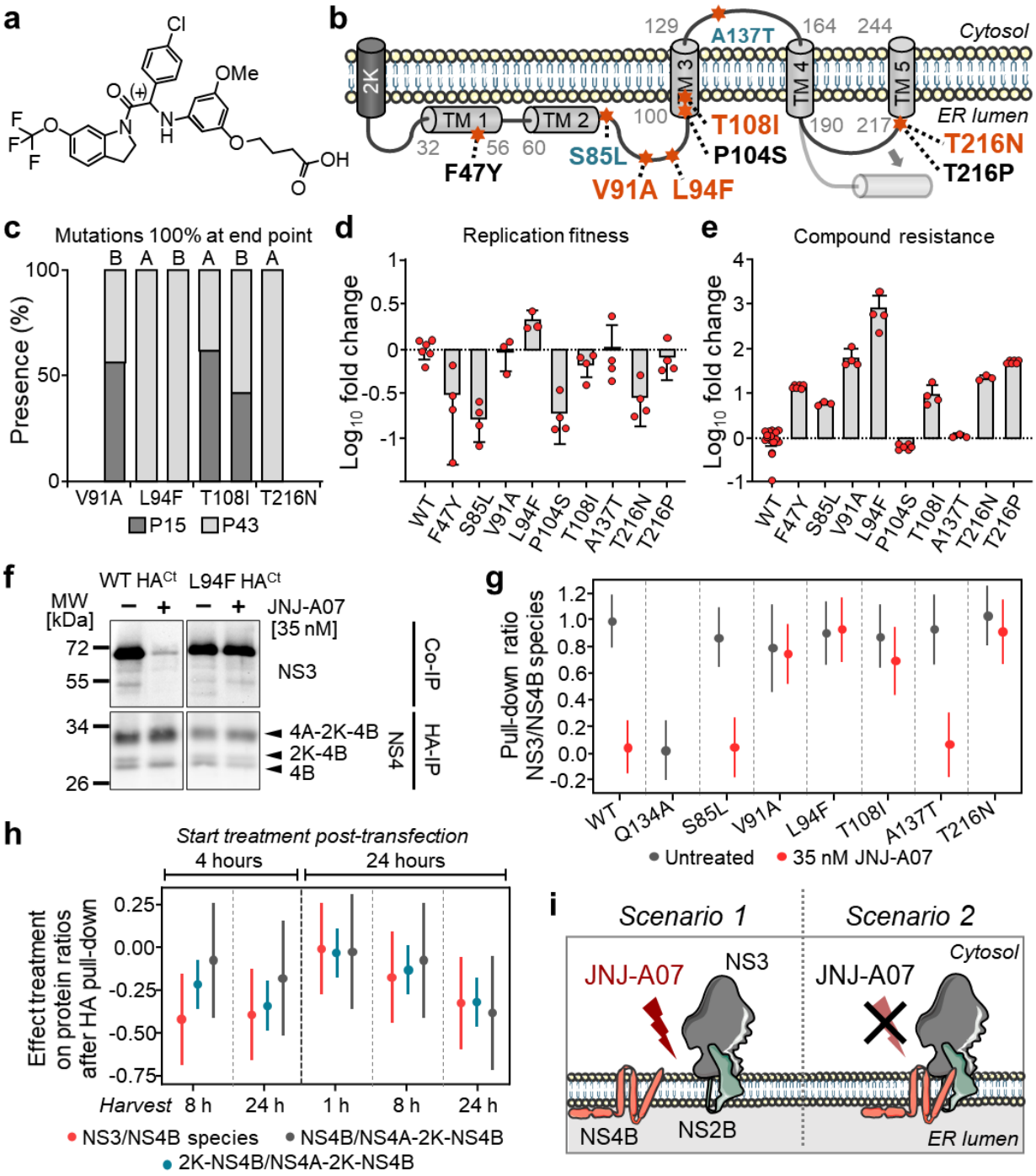

1073 **Figure 2**

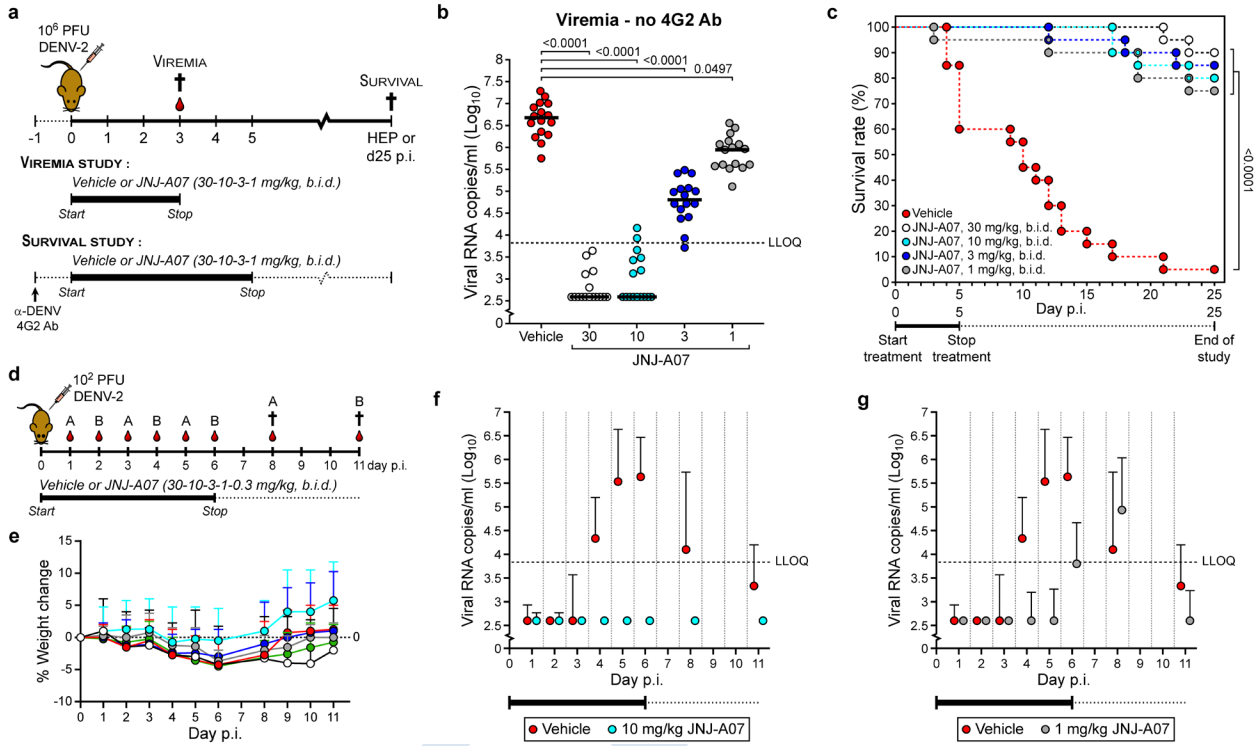

1075 **Figure 3**

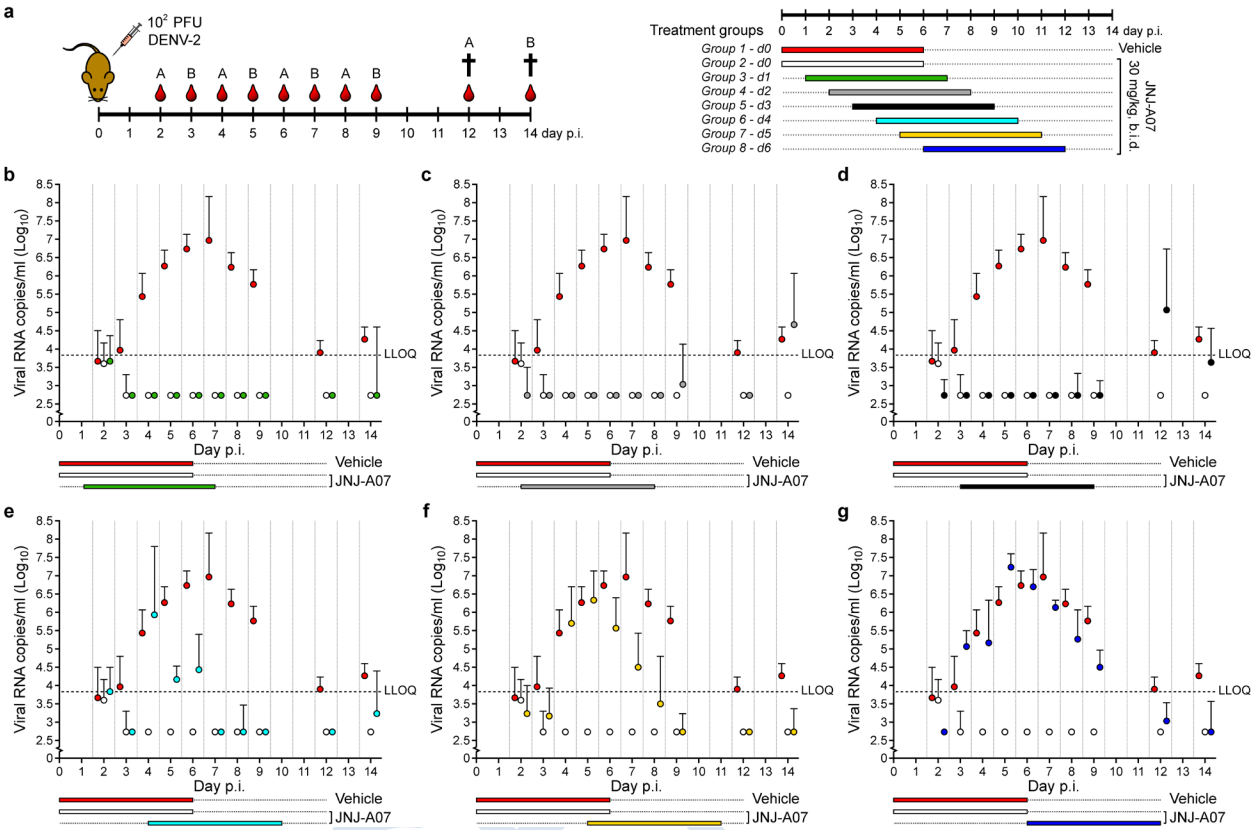

1077 **Extended Data Figure 1**

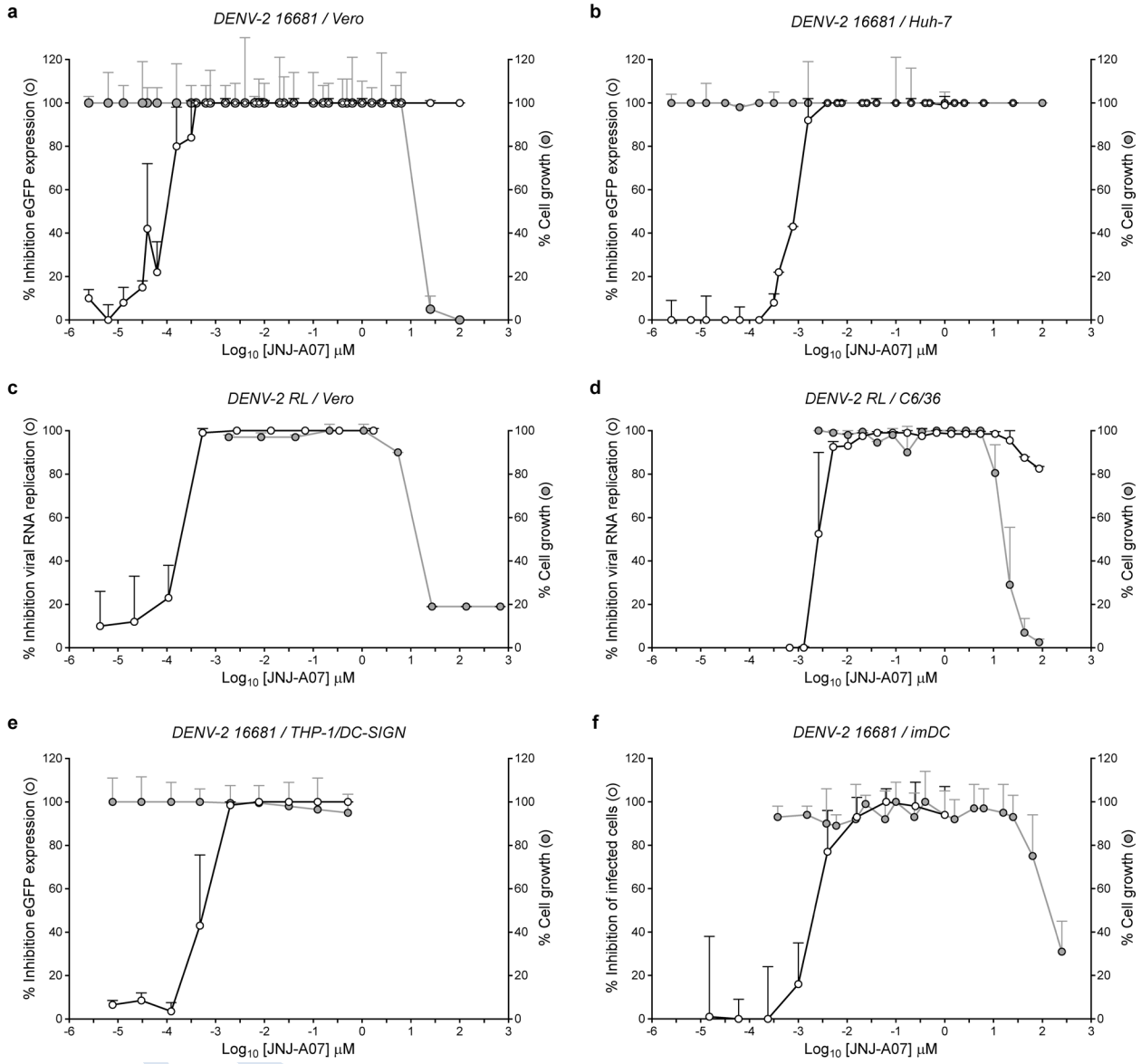

# Extended Data Figure 2

**a**

**Antiviral activity of JNJ-A07 against various RNA and DNA viruses**

| Virus | Strain | Cells | Antiviral $EC_{50}$ (μM) | Toxicity $CC_{50}$ (μM) | SI* |
|---|---|---|---|---|---|
| CHIKV | S27 | Huh-7 | 23 | >25 | >1 |
| HAdV | C, type 5 | HeLa | NA† | 6.8 | / |
| HBV | Genotype D | HepG2.117 | >22‡ | 22 | <1 |
| HCV | Genotype 1b | Huh-7-Luc§ | 65 | >100‖ | >2 |
| HIV | IIIB | MAGI-CCR5 | 5.5 | 33 | 6 |
| hRV | A16 | HeLa | NA† | 13 | / |
| hRV | B14 | HeLa | NA† | 9.1 | / |
| IVA | Taiwan/1/86 (H1N1) | MDCK | >3.6‡ | 3.6 | <1 |
| IVA | PR8/1934 (H1N1) | MDCK | >3.6‡ | 3.6 | <1 |
| IVB | Singapore | MDCK | >3.6‡ | 3.6 | <1 |
| RSV | rgRSV224 | HeLa | 19 | 52 | 3 |
| rVSV | Indiana | A549 | 57 | >90 | >2 |
| VACV | Western reserve 56 | Vero E6 | 35 | 45 | 1 |
| JEV | CNS769-Laos | Vero E6 | >5.0 | ND | / |
| WNV | USA | Vero E6 | >5.0 | ND | / |
| YFV | Bolivia | Vero E6 | 1.8 | ND | / |
| ZIKV | H/PF/2013 | Vero E6 | 4.8 | ND | / |

*Selectivity index (SI) was calculated by dividing the average $CC_{50}$ value by the average $EC_{50}$ value.
†Not approved because any sign of antiviral activity was associated with toxicity.
‡In case the $EC_{50}$ value was higher than the $CC_{50}$ value, the $EC_{50}$ value was set at $>CC_{50}$.
§Huh-7-Luc are HCV-Luc replicon containing cells.
‖Huh-7-CMV-Luc cells were used to measure the toxicity of the compound.

**b**

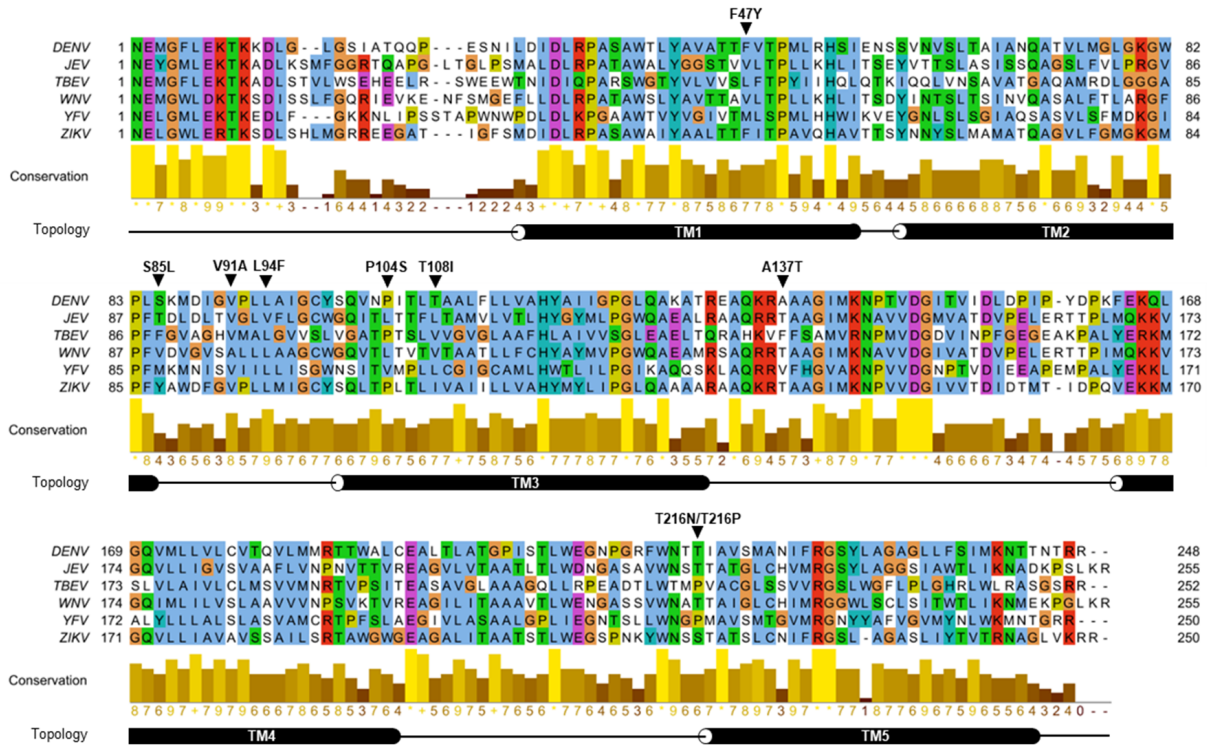

# Extended Data Figure 3

a

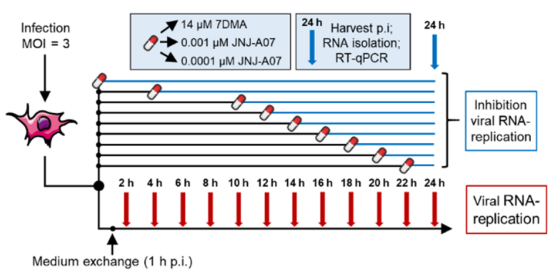


b

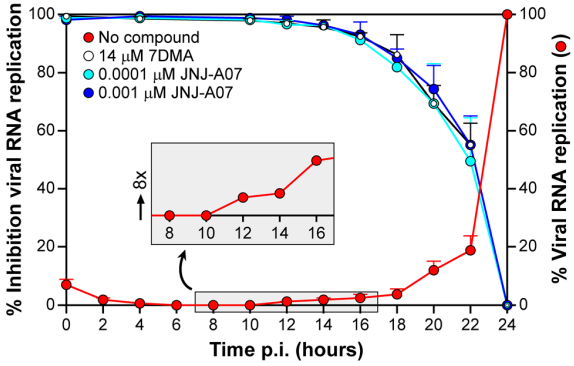


c

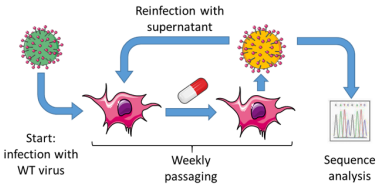


d

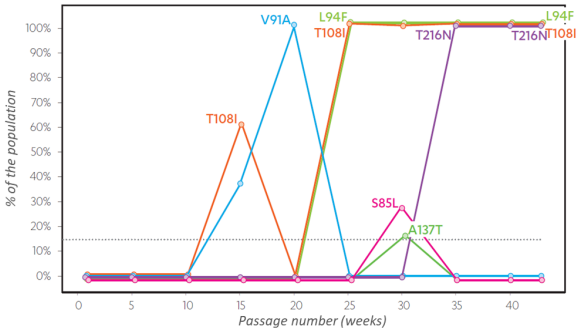


| $EC_{50}$ µM | 0.00007 | 0.0001 | 0.0001 | 0.002 | 0.005 | 0.05 | 0.5 | 3.8 | 3.8 | 3.8 |
|---|---|---|---|---|---|---|---|---|---|---|

e

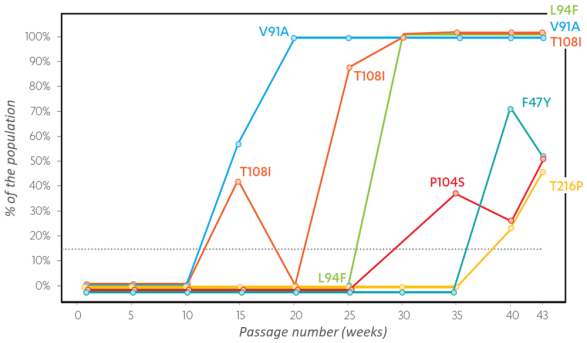


| $EC_{50}$ µM | 0.00007 | 0.0001 | 0.0003 | 0.002 | 0.005 | 0.02 | 0.5 | 0.9 | 3.8 | 3.8 |
|---|---|---|---|---|---|---|---|---|---|---|

f

**NS4B mutations in DENV mutant variants at end point**

| Compound name | Mutation in NS4B | Endpoint |
|---|---|---|
| JNJ-A07, sample A | L94F, T108I, T216N | Passage 43 |
| JNJ-A07, sample B | F47Y (52%), V91A, L94F, T108I, P104S (51%), T216P (46%) | Passage 43 |
| Analogue 1, sample A | V91A, L94F (20%), T108I | Passage 29 |
| Analogue 1, sample B | L94F, T108I | Passage 29 |

One passage represents one week.

g

**Natural occurrence of the NS4B mutations in clinical isolates**

| NS4B mutation | Frequency mutant in clinical isolates* |
|---|---|
| None (WT) | |
| F47Y | 0% |
| S85L | 0% |
| V91A | 1.3% (DENV-2), 0.4% (DENV-3) |
| L94F | 0% |
| P104S | 0% |
| T108I | 0.12% (DENV-1), 0.9% (DENV-2), 2.6% (DENV-4) |
| A137T | 3.5% (DENV-2), 100% in other serotypes |
| T216N | 0% |
| T216P | 0% |

*The natural occurrence of the mutations was retrieved from the Virus Pathogen Resource database (www.viprbrc.org; accessed in May 2020). Prevalence values ≤0.1% are not shown.

1083 # Extended Data Figure 4

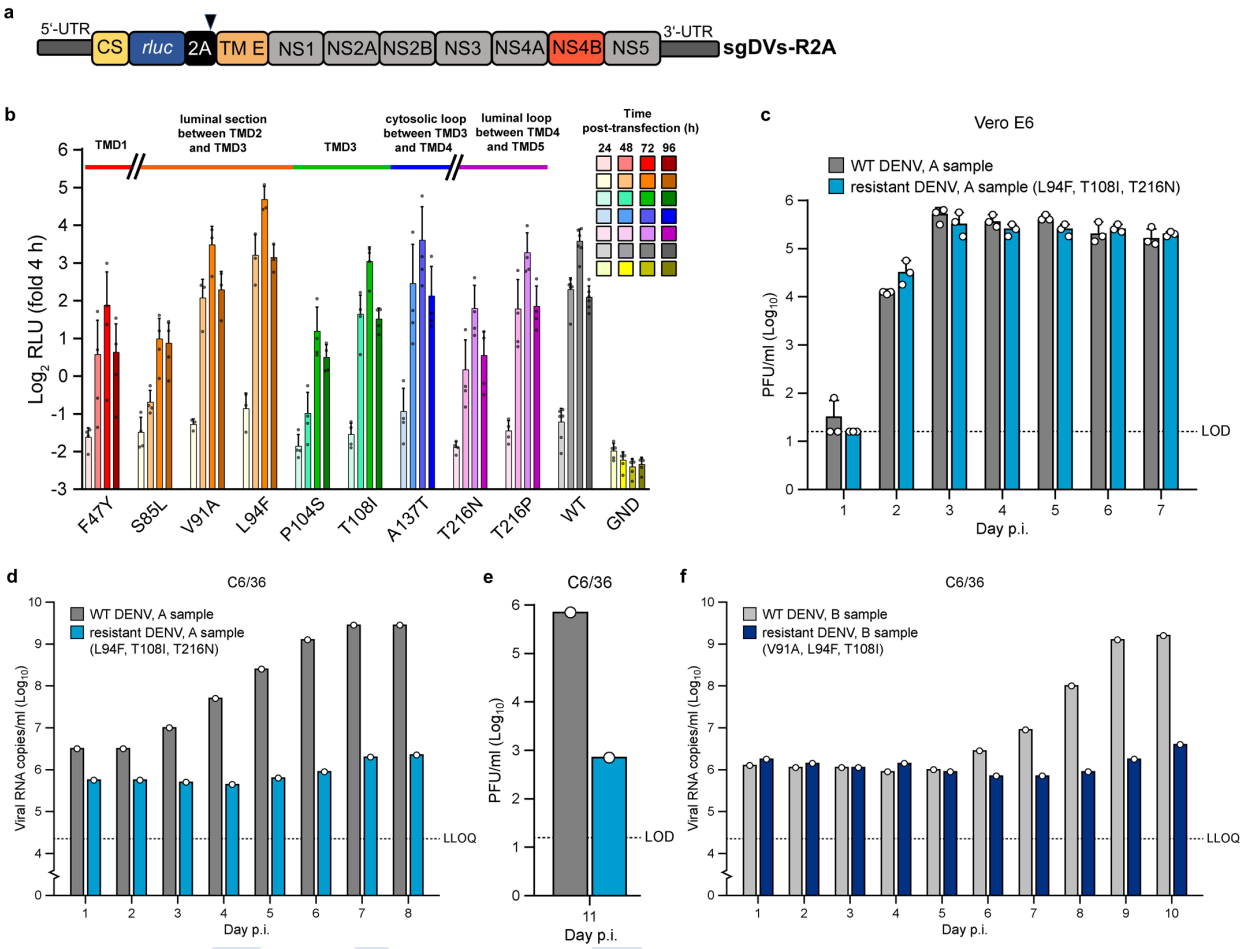

# Extended Data Figure 5

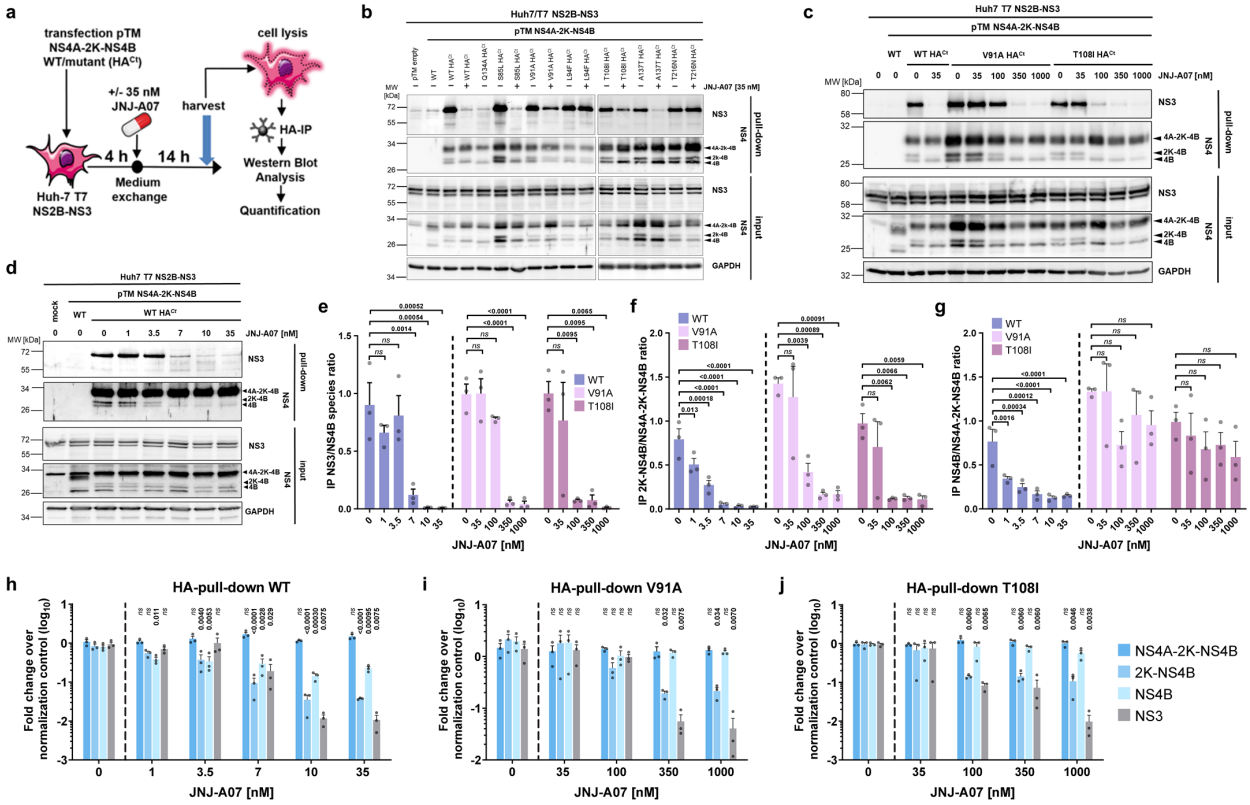


**k** Fold change in $EC_{50}$

| | $EC_{50}$ (µM) NS3/NS4B species | Fold change NS3/NS4B species | $EC_{50}$ (µM) 2K-NS4B/ NS4A-2K-NS4B | Fold change 2K-NS4B/ NS4A-2K-NS4B |
|---|---|---|---|---|
| WT | 0.006 ± 0.0007 | 1 | 0.008 ± 0.002 | 1 |
| V91A | 0.2 ± 0.03 | 42 | 0.1 ± 0.01 | 15 |
| T108I | 0.05 ± 0.03 | 9 | 0.04 ± 0.02 | 5 |

NS4B species are the combined signal intensities of NS4A-2K-NS4B, 2K-NS4B and NS4B.

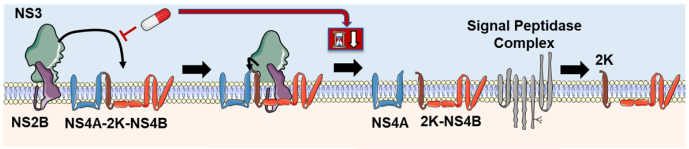

1087 # Extended Data Figure 6

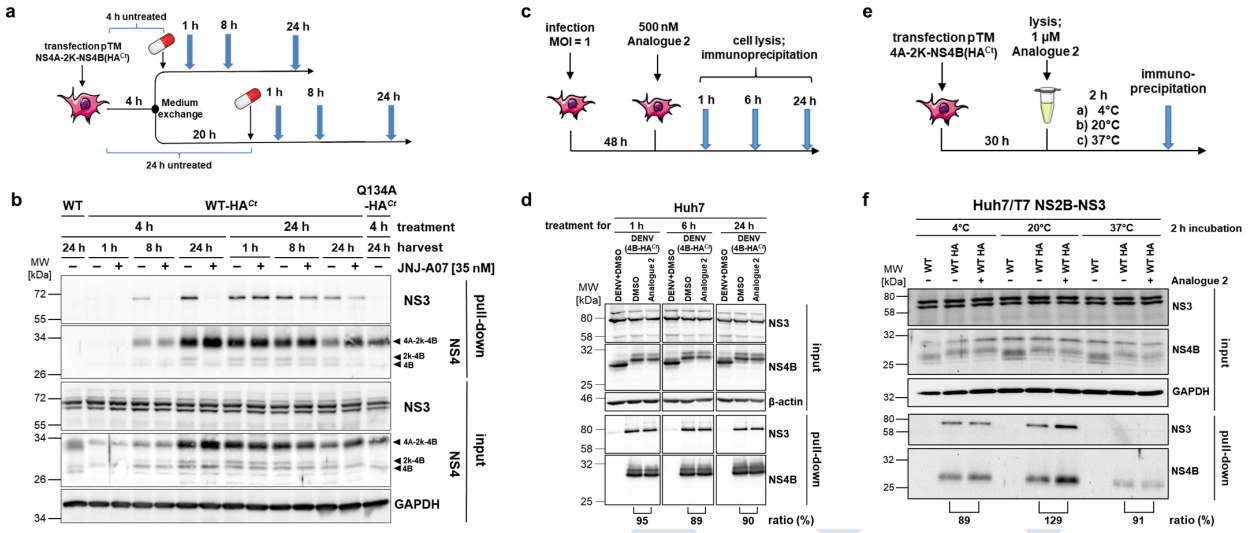

1089 **Extended Data Figure 7**

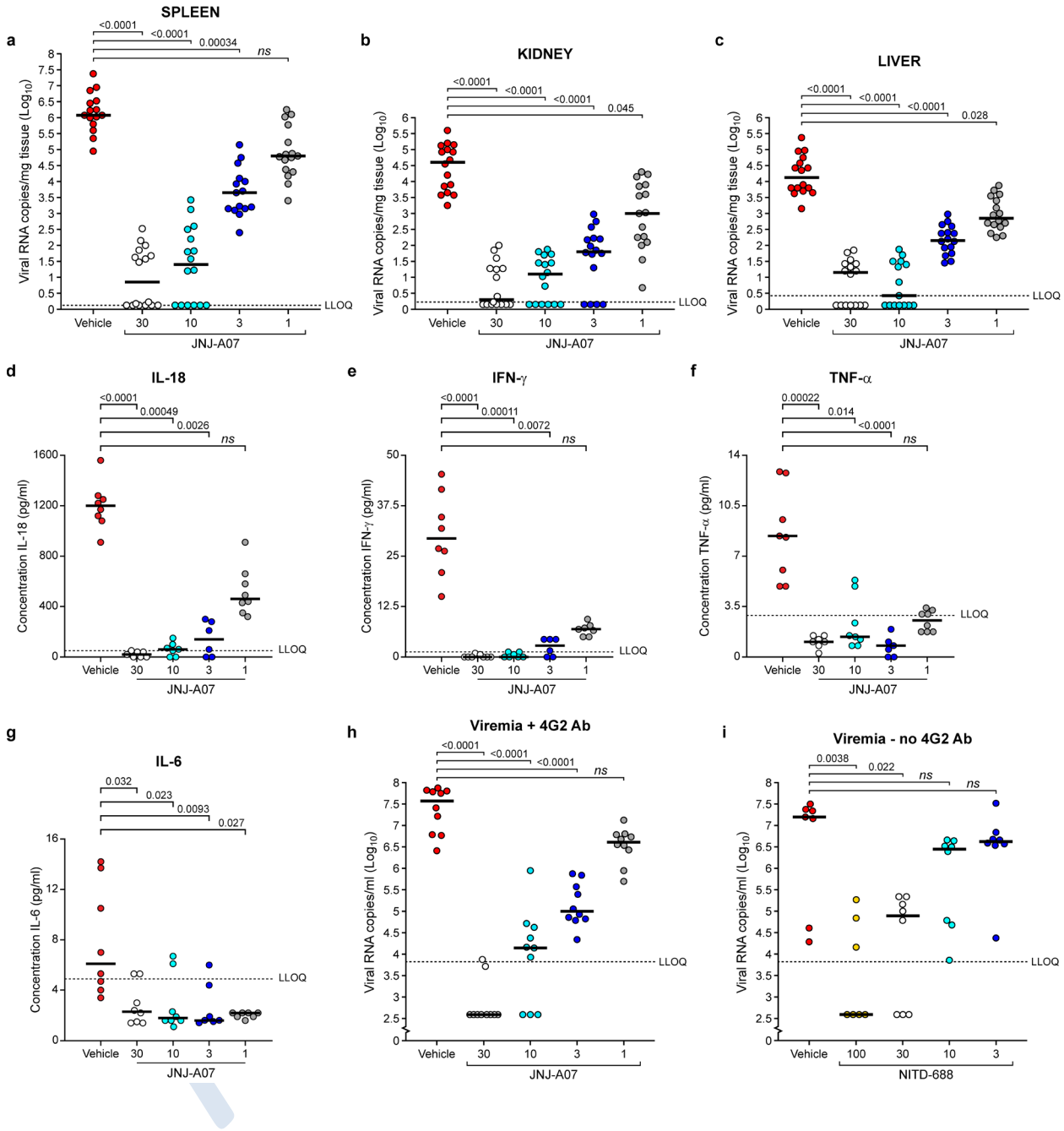

1091 **Extended Data Figure 8**

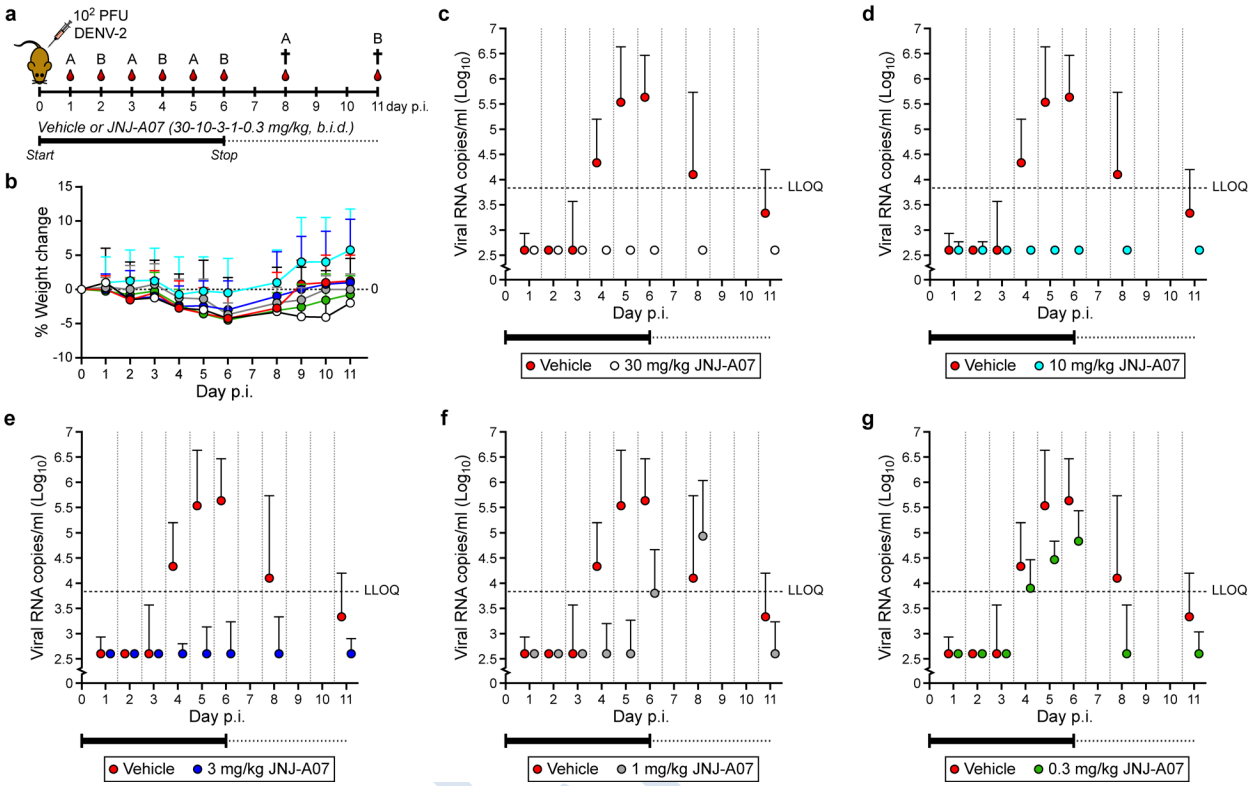

1093 **Extended Data Table 1**

| Compound | Structure | Antiviral $EC_{50}$ (μM) | Toxicity $CC_{50}$ (μM) | SI* |
|---|---|---|---|---|
| JNJ-A07 | 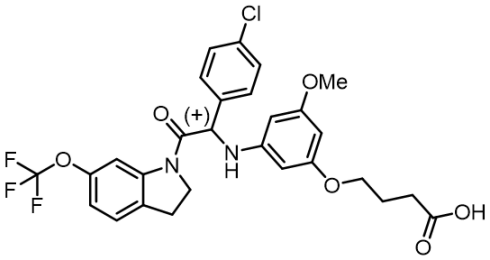 | 0.0001 ± 0.00007 | 13 ± 1.1 | 130,000 |
| Analogue 1 | 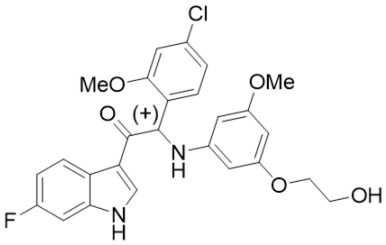 | 0.001 ± 0.0002 | 4.7 ± 0.9 | 4,700 |
| Analogue 2 | 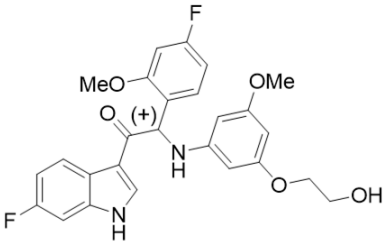 | 0.004 ± 0.001 | 8.6 ± 1.8 | 2,150 |
| NITD-688 | 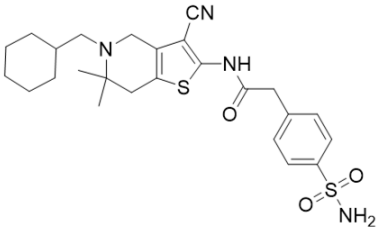 | 0.09 ± 0.07 | >41 ± 13 | >456 |

1095 # Extended Data Table 2

**a**

| | Dose 2.5 mg/kg | |
|---|---|---|
| | **Mouse** | **Rat** |
| $CL_p$ (mL/min/kg) | 4.1 ± 0.4 | 4.4 ± 2.5 |
| $V_{dssp}$ (L/kg) | 0.78 ± 0.04 | 1.0 ± 0.4 |
| $t_{1/2}$ (h) | 3.0 ± 0.04 | 3.1 ± 0.3 |
| $AUC_{(0\text{-last})}$ (ng.h/mL) | 10,227 ± 903 | 11,327 ± 5,160 |
| $AUC_{(0\text{-inf})}$ (ng.h/mL) | 10,250 ± 908 | 11,380 ± 5,200 |

**b**

| | Dose in mice | | | | Dose in rats |
|---|---|---|---|---|---|
| | **1 mg/kg** | **3 mg/kg** | **10 mg/kg** | **30 mg/kg** | **10 mg/kg** |
| $C_{max}$ (ng/mL) | 280 ± 101 | 834 ± 265 | 2,087 ± 235 | 12,143 ± 4,500 | 4,440 ± 322 |
| $T_{max}$ (h) | 1.3 ± 0.6 | 2.3 ± 1.5 | 1.2 ± 0.8 | 2.0 ± 1.7 | 5.0 ± 1.7 |
| $AUC_{(0\text{-last})}$ (ng.h/mL) | 1,469 ± 404 | 6,980 ± 994 | 15,804 ± 872 | 71,963 ± 8,550 | 61,806 ± 3,853 |
| Last time point (h) | 7 (*n*=1), 24 (*n*=2) | 24 | 24 | 24 | ND |
| $AUC_{(0\text{-inf})}$ (ng.h/mL) | 1,522 ± 330 | 6,994 ± 997 | 15,858 ± 855 | 72,132 ± 8,590 | 62,034 ± 3,694 |
| F (%) | 37 ± 8.1 | 57 ± 8.1 | 39 ± 2.1 | 59 ± 7.0 | >100% |
| MTD (mg/kg) | ND | ND | ND | ND | 1,000 |